Cellular/Molecular

# Novel $G\alpha_S$-Protein Signaling Associated with Membrane-Tethered Amyloid Precursor Protein Intracellular Domain

**Carole Deyts,[1] Kulandaivelu S. Vetrivel,[1] Shibandri Das,[1] Yumiko M. Shepherd,[1] Denis J. Dupré,[4] Gopal Thinakaran,[1,2,3] and Angèle T. Parent[1]**

Departments of [1]Neurobiology, [2]Neurology, and [3]Pathology, The University of Chicago, Chicago, Illinois 60637, and [4]Department of Pharmacology, Dalhousie University, Halifax, Nova Scotia B3H 4R2, Canada

**Numerous physiological functions, including a role as a cell surface receptor, have been ascribed to Alzheimer's disease-associated amyloid precursor protein (APP). However, detailed analysis of intracellular signaling mediated by APP in neurons has been lacking. Here, we characterized intrinsic signaling associated with membrane-bound APP C-terminal fragments, which are generated following APP ectodomain release by $\alpha$- or $\beta$-secretase cleavage. We found that accumulation of APP C-terminal fragments or expression of membrane-tethered APP intracellular domain results in adenylate cyclase-dependent activation of PKA (protein kinase A) and inhibition of GSK3$\beta$ signaling cascades, and enhancement of axodendritic arborization in rat immortalized hippocampal neurons, mouse primary cortical neurons, and mouse neuroblastoma. We discovered an interaction between BBXXB motif of APP intracellular domain and the heterotrimeric G-protein subunit $G\alpha_S$, and demonstrate that $G\alpha_S$ coupling to adenylate cyclase mediates membrane-tethered APP intracellular domain-induced neurite outgrowth. Our study provides clear evidence that APP intracellular domain can have a nontranscriptional role in regulating neurite outgrowth through its membrane association. The novel functional coupling of membrane-bound APP C-terminal fragments with $G\alpha_S$ signaling identified in this study could impact several brain functions such as synaptic plasticity and memory formation.**

## Introduction

Alzheimer's disease (AD) is pathologically characterized by the cerebral deposition of $\beta$-amyloid peptides (A$\beta$) in senile plaques. A$\beta$ is released by the sequential proteolytic processing of amyloid precursor protein (APP), a type I transmembrane protein. Cleavage of full-length APP (APP-FL) by $\alpha$- or $\beta$-secretase releases the entire ectodomain, leaving behind membrane bound C-terminal fragments (APP-CTF), made of the transmembrane and cytoplasmic domains (Lichtenthaler et al., 2011). While APP metabolism and contribution of A$\beta$ to AD pathology has been the focus of intense investigation, the normal biological function(s) of APP in the nervous system are still not completely understood (Turner et al., 2003; Thinakaran and Koo, 2008; Guo et al., 2012). It has been proposed that APP can affect synaptic function by its dual roles via its cell-adhesive properties or through its putative receptor-like intracellular signaling (Ando et al., 1999; Turner et al., 2003; Soba et al., 2005; Thinakaran and Koo, 2008). Moreover, several lines of evidence reveal that APP expression modulates neurite outgrowth in neuroblastoma cells and neurons (Allinquant et al., 1995; Perez et al., 1997; Ando et al., 1999; Small et al., 1999; Leyssen et al., 2005; Young-Pearse et al., 2008; Hoe et al., 2009). Mice lacking APP expression show progressive loss of presynaptic terminals, reduced dendritic length, impairment of synaptic plasticity, and deficit in learning and memory (Turner et al., 2003; Zheng and Koo, 2006; Aydin et al., 2012; Guo et al., 2012; Hoe et al., 2012). However, the molecular mechanisms underlying the above observations largely remain undefined.

APP cytosolic domain possesses conserved sequence motifs responsible for complex network of protein–protein interactions (Müller et al., 2008; Suzuki and Nakaya, 2008; Schettini et al., 2010; Aydin et al., 2012), which could account for a variety of cellular functions mediated by APP. The present work focuses on the modulation of APP cytosolic tail-mediated intracellular signaling, which underlies neurite outgrowth. We have designed a membrane-tethered APP intracellular domain construct (referred to as mAICD) to allow us to activate, in a constitutive manner, putative signaling associated with APP-CTF. We report here that accumulation of APP-CTF or membrane tethering of APP cytosolic sequence stimulates neurite outgrowth in mouse N2a neuroblastoma cells, rat H19-7 immortalized hippocampal cells, and mouse cortical primary neurons. Expression of mAICD

Received Oct. 27, 2011; accepted Nov. 29, 2011.

Author contributions: C.D., D.J.D., G.T., and A.T.P. designed research; C.D., K.S.V., S.D., and Y.M.S. performed research; D.J.D. contributed unpublished reagents/analytic tools; C.D., K.S.V., and A.T.P. analyzed data; C.D., G.T., and A.T.P. wrote the paper.

This work was supported by National Institutes of Health Grants NS055223 (A.T.P.) and AG019070 (G.T.), and Alzheimer's Association Grant IIRG-06-26148 (A.T.P.). We thank Dr. Mitchell Villereal for providing H19-7 cells. We are grateful to Stacy Herrera, Breanne Kassarjian, Rafael Marquez, and Megan Rawson for technical assistance. We thank Drs. Eric Norstrom and Hyun-Ju Kim, and members of the Thinakaran Laboratory for helpful discussions and advice.

The authors declare no competing financial interests.

Correspondence should be addressed to Angèle T. Parent, Department of Neurobiology, The University of Chicago, 924 East 57th Street, Chicago, IL 60637. E-mail: aparent@uchicago.edu.

DOI:10.1523/JNEUROSCI.5433-11.2012

 0270-6474/12/321714-16$15.00/0

initiates a previously unrecognized signaling pathway that involves a novel association between APP intracellular domain and the heterotrimeric G-protein subunit $G\alpha_S$. This functional coupling leads to steady-state increase of phosphorylated protein kinase A (PKA) substrates such as CREB and GSK3$\beta$, which are likely to impact neuronal morphology and function.

## Materials and Methods

*Reagents.* Compound E was generously provided by Dr. Todd E. Golde (University of Florida, Gainesville, FL) (Seiffert et al., 2000). (5*R*,6*S*,8*S*)-Hexyl 6-hydroxy-5-methyl-13-oxo-6,7,8,13,14,15-hexahydro-5*H*-16-oxa-4b, 8a,14-triaza-5,8-methanodibenzo[*b*,*h*]cycloocta[*jkl*]cyclopenta[*e*]-asindacene-6-carboxylate (KT5720) and *cis*-*N*-(2-phenylcyclopentyl)-azacyclotridec-1-en-2-amine (MDL-12,330A) were obtained from BIOMOL. Tetrodotoxin was purchased from Alomone Labs. Cell culture and transfection reagents were purchased from Invitrogen. Unless indicated, all other reagents were purchased from Sigma-Aldrich.

*Antibodies.* Rabbit polyclonal antibodies CT11, CTM1, and PS1NT have been described previously (von Koch et al., 1997; Thinakaran et al., 1998; Vetrivel et al., 2009). The following antibodies were purchased from commercial sources: polyclonal phospho-(Ser$^{133}$) CREB, polyclonal phospho-(Ser$^{9}$) GSK3$\beta$, and goat anti-mouse CD147 (clone T-18) (Santa Cruz Biotechnology); mAb HA (clone 6E2) and polyclonal phospho-(Ser/Thr) PKA antibody (Cell Signaling Technology); mAb anti-HA (clone 12CA5) (Roche Diagnostics); polyclonal anti-MAP2 and mAb anti-Flag (clone F3165) (Sigma-Aldrich); mAb GAPDH (Abcam); polyclonal dimethyl histone H3 (Arg$^{17}$) (Millipore Bioscience Research Reagents); and mAb 82E1, which recognizes an epitope within residues 1–16 of A$\beta$ (IBL International). Alexa 488- and Alexa 555-conjugated secondary antibodies were purchased from Invitrogen. IRDye 680 and IRDye 800CW-conjugated secondary antibodies were purchased from LI-COR Biosciences.

*Cell cultures.* Mouse N2a neuroblastoma cells were cultured in 1:1 DMEM–Opti-MEM medium supplemented with 5% fetal bovine serum. N2a pools stably expressing mAICD, PS1-wt, and PS1-D385A, or harboring an empty vector (EV), were generated by retroviral infections as described previously (Onishi et al., 1996; Vetrivel et al., 2009). Briefly, retroviral supernatants collected 48 h after transfection of Plat-E cells were used to infect N2a cells in the presence of 8 $\mu$g/ml polybrene. Stably transduced cells were selected in the presence of 1 $\mu$g/ml puromycin and pooled for further analysis. H19-7 rat embryonic immortalized hippocampal cell line was cultured in DMEM supplemented with 10% fetal bovine serum (FBS) at 33°C as described previously (Eves et al., 1992; Wu et al., 2004). Immediately after transfection, proliferating H19-7 cells were incubated at 39°C in a supplemented DMEM containing 50 ng/ml basic fibroblast growth factor to initiate differentiation and neurite outgrowth (Eves et al., 1992; Wu et al., 2004). COS cells were maintained in DMEM supplemented with 10% FBS. Primary cultures of cortical neurons were generated from E16 male and female embryos as described previously (Parent et al., 2005) and maintained at 37°C in Minimal Essential Medium supplemented with 1% glutamine, 5% horse serum, 0.5% D-glucose, 0.15% $HCO_3$, and nutrients, in a humidified 10% $CO_2$ incubator. N2a and H19-7 were grown in six-well plates on a poly-L-lysine-coated 18 mm glass coverslips, whereas cortical neurons were cultured on 0.1% polyethylenimine-coated glass coverslips. N2a and H19-7 cells were transiently transfected using LipoD293 according to manufacturer's protocol (SignaGen Laboratories). Transient transfection of 7–11 DIV neurons was performed in Neurobasal medium using Lipofectamine 2000. After 3 h, transfection medium was replaced by 50% original medium and 50% supplemented Minimal Essential Medium without serum. Sixteen to 24 h after transfection, cells were treated with Compound E (10 nM) and/or various drugs, and cultured for another 24 h before analysis.

*Expression plasmids.* Overlap extension PCR was used to generate a cDNA that encodes mAICD or mALID1 by replacing the extracellular and transmembrane domains of APP or APLP1 with the sequence encoding the membrane-targeting MyrPalm motif of the Src family tyrosine kinase Lyn (MGCIKSKRKDNLNDDGVDN). The C terminus of mAICD was tagged with CT11 epitope (RFLEERP) of APLP1 (von Koch et al., 1997). Similarly, sequences encoding CT11-tagged C-terminal 50 residues of APP (AICD) was generated by overlap PCR. The resulting cDNAs were cloned into pMXpuro retroviral vector (kindly provided by Dr. Toshio Kitamura, University of Tokyo, Tokyo, Japan). To generate membrane-tethered control construct (mCtl), the 47 aa APP intracellular domain in mAICD was replaced with residues 1–47 of the cyan fluorescent protein. To generate mAICD-mutAAA, the residues RHLSK (corresponding to amino acids 672–676 of $APP_{695}$) in mAICD were mutated to AALSA. PCR amplified regions in all constructs were verified by sequencing. APP-C99–6Myc (a gift from Dr. Alison Goate, Washington University, St. Louis, MO), APP-FL, APP $\alpha$-site cleavage mutant (APP-F615P; numbering corresponds to $APP_{695}$), $\beta$-site cleavage mutant (APP-M596V) were generated by PCR mutagenesis. Plasmids encoding HA-$G\alpha_S$-wt and palmitoylation-deficient HA-$G\alpha_S$-C3S have been described previously (Wedegaertner et al., 1993; Dupré et al., 2007). Plasmids encoding Flag epitope-tagged dopamine $D_1$ receptor (plasmid 15464) and $\beta$1 adrenergic receptor (plasmid 14698) were obtained from Addgene.

*Protein analysis.* Total cell lysates for immunoblotting were prepared in 150 mM NaCl, 50 mM Tris-HCl, pH 7.4, 0.5% NP-40, 0.5% sodium deoxycholate, 5 mM EDTA, 0.25% SDS, 0.25 mM phenylmethylsulfonyl fluoride, and a protease inhibitor mixture (Sigma-Aldrich), and briefly sonicated on ice. Coimmunoprecipitation was modified from previously described protocols (Biederer et al., 2002; Gong et al., 2010). Briefly, cells were lysed in ice-cold lysis buffer (25 mM HEPES, pH 7.4; 5 mM $MgCl_2$, 1% NP-40, 125 mM potassium acetate, 10% glycerol, and protease inhibitor mixture). Lysates were clarified by centrifugation at 13,000 rpm for 20 min at 4°C, and aliquots of the supernatants were adjusted to 500 $\mu$l with lysis buffer and incubated overnight with the indicated antibodies at 4°C. Immune complexes were captured by incubating with 40 $\mu$l of protein G-agarose beads (Thermo Fisher Scientific) for 2 h at 4°C, and washed three times with 500 $\mu$l of lysis buffer at 4°C. Bound proteins were eluted in Laemmli buffer and analyzed by immunoblotting along with an aliquot of the total input lysate.

*Subcellular fractionation.* N2a cells were homogenized in buffer A, containing 5 mM HEPES, 1.5 mM $MgCl_2$, 10 mM KCl, 0.125% Triton, 0.25 mM phenylmethylsulfonyl fluoride, and protease inhibitor mixture at pH 7.9, and centrifuged at 1000 × *g* for 10 min. The nuclear pellet (P1) was washed with buffer B, containing 20 mM HEPES, 25% glycerol, 0.5 mM NaCl, 0.5 mM $MgCl_2$, 0.5 mM EDTA, 0.25% Triton X-100, 0.25 mM PMSF, and protease inhibitor mixture, and subsequently sonicated. The supernatant was centrifuged at 114,000 × *g* for 30 min to yield a membrane pellet (P2) and supernatant (S2) containing soluble cytosolic proteins. Each fraction was resuspended in equal volume of buffer B and analyzed by immunoblotting with CT11 antibody. Histone H3, CD147, and GAPDH were used as nuclear, membrane, and cytosolic markers, respectively. Lipid rafts from cultured cells were isolated as described previously (Vetrivel et al., 2004). Briefly, cells were lysed on ice in a buffer containing 0.5% Lubrol WX (Lubrol 17A17; Serva), and lysates were subject to centrifugation on discontinuous flotation density gradients and aliquot of fractions were analyzed by Western blotting.

*Immunofluorescence staining.* Cells were maintained for 3 h in HEPES buffer before forskolin (FSK) stimulation (50 $\mu$M, 30 min at 37°C), as previously described (Barnes et al., 2008). To reduce neuronal activity, cortical cultures were serum deprived for 3 h using HEPES buffer supplemented with tetrodotoxin (1 $\mu$M). To examine the signaling cascade activation, pharmacological inhibitors were added 30 min before FSK stimulation (2 $\mu$M KT5720 or 10 nM MDL-12,330A). To stimulate or inhibit neurite extension, cells were exposed to 1 $\mu$M FSK, 10 nM MDL-12,330A, or 10 nM Compound E for 24 h. Following the treatment, cells were fixed for 30 min at 4°C with 4% paraformaldehyde/4% sucrose and permeabilized on ice with 0.2% Triton X-100 solution for 8 min. Fixed cells were incubated overnight at 4°C with antibodies of interest [1: 20,000 CT11, 1:100 phospho-(Ser/Thr) PKA, 1:100 phospho-(Ser$^{133}$) CREB, 1:250 phospho-(Ser$^{9}$) GSK3$\beta$, 1:5000 MAP2, 1:5000 HA clone 6E2]. Subsequently, cells were incubated with Alexa 488- and Alexa 555-conjugated secondary antibodies (1:250) for 1 h at room temperature,

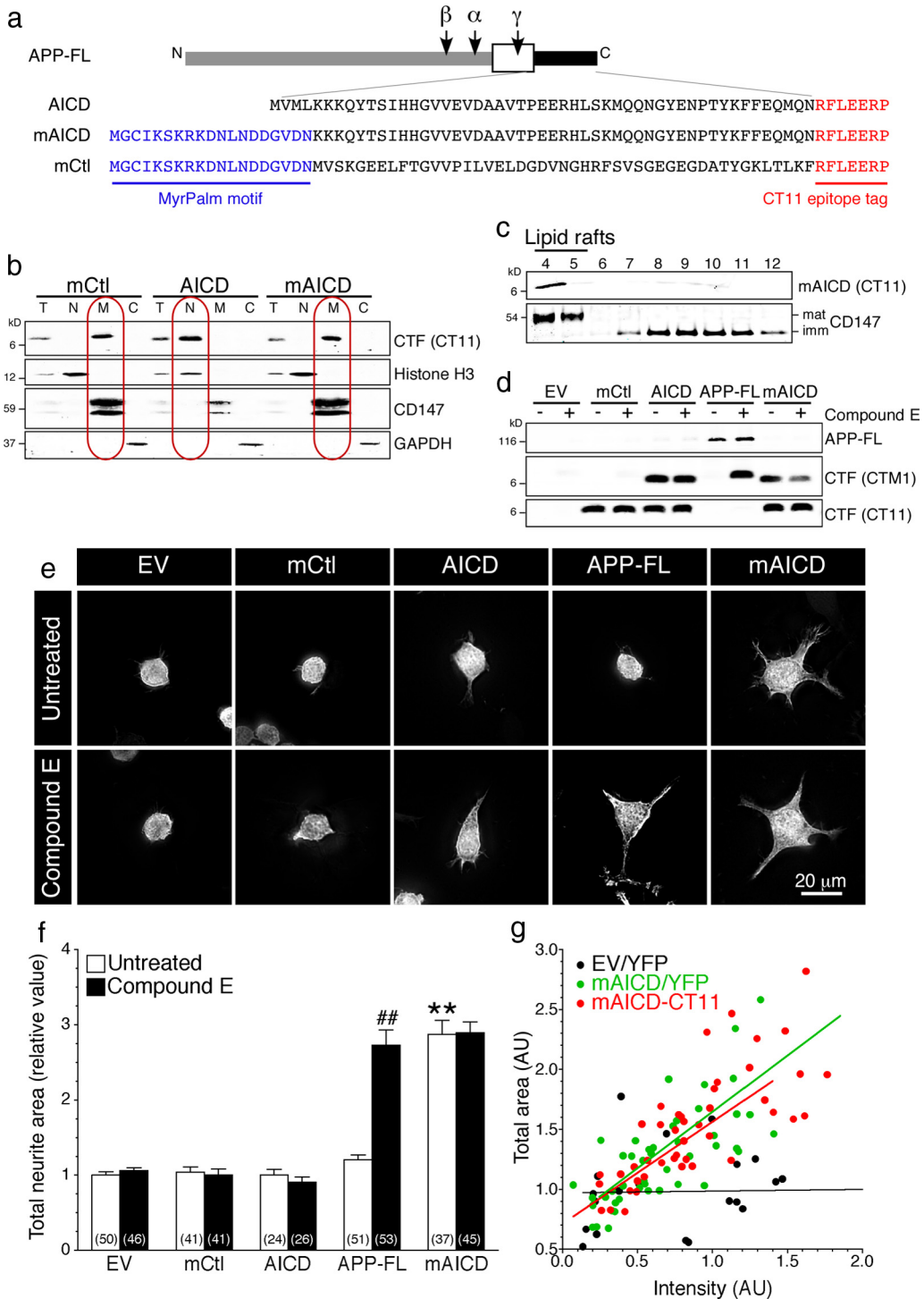


**Figure 1.** Accumulation of membrane-bound APP intracellular domain enhances neurite outgrowth in N2a cells. ***a***, Schematic representation of full-length and C-terminal APP constructs. ***b***, Analysis of mCtl, AICD, and mAICD distribution by subcellular fractionation of total lysates (T). Histone H3, CD147, and GAPDH were used as markers for nuclear (N), membrane (M), and cytosolic (C) fractions, respectively. ***c***, Sucrose density gradient fractionation of lipid rafts in N2a pools stably expressing mAICD. Detergent-insoluble membrane proteins are enriched in fractions 4–5 marked by mature CD147 protein and flotillin-2 (data not shown), whereas detergent-soluble membrane proteins are found in 8–12 fractions marked by immature CD147 protein (Vetrivel et al., 2004, 2008). ***d***, Immunoblot analysis of transfected cells without or after treatment with Compound E (10 nM; 24 h). CT11 antibody recognizes CT11 epitope-tagged polypeptides, whereas CTM1 detects the C terminus of APP (von Koch et al., 1997; Vetrivel et al., 2009). ***e***, YFP fluorescence images of N2a cells cotransfected with YFP and the indicated plasmids. ***f***, Quantitative analysis of total neurite area relative to EV cells quantified from *z*-stack images. ***g***, Correlation analysis between the total area and mAICD expression quantified by CT11 immunostaining (red circles) or cotransfected YFP fluorescence intensity (green circles). The black circles represent analysis of cells cotransfected with YFP and EV. Statistical analysis was performed using ANOVA Kruskal–Wallis test followed by Dunn's *post hoc* multiple-comparison analysis. The total number of cells quantified is shown in parentheses. $^{**}p < 0.001$, compared with EV-transfected cells, and $^{\#\#}p < 0.001$, Compound E-treated cells compared with untreated cells in each case. Error bars indicate SEM.

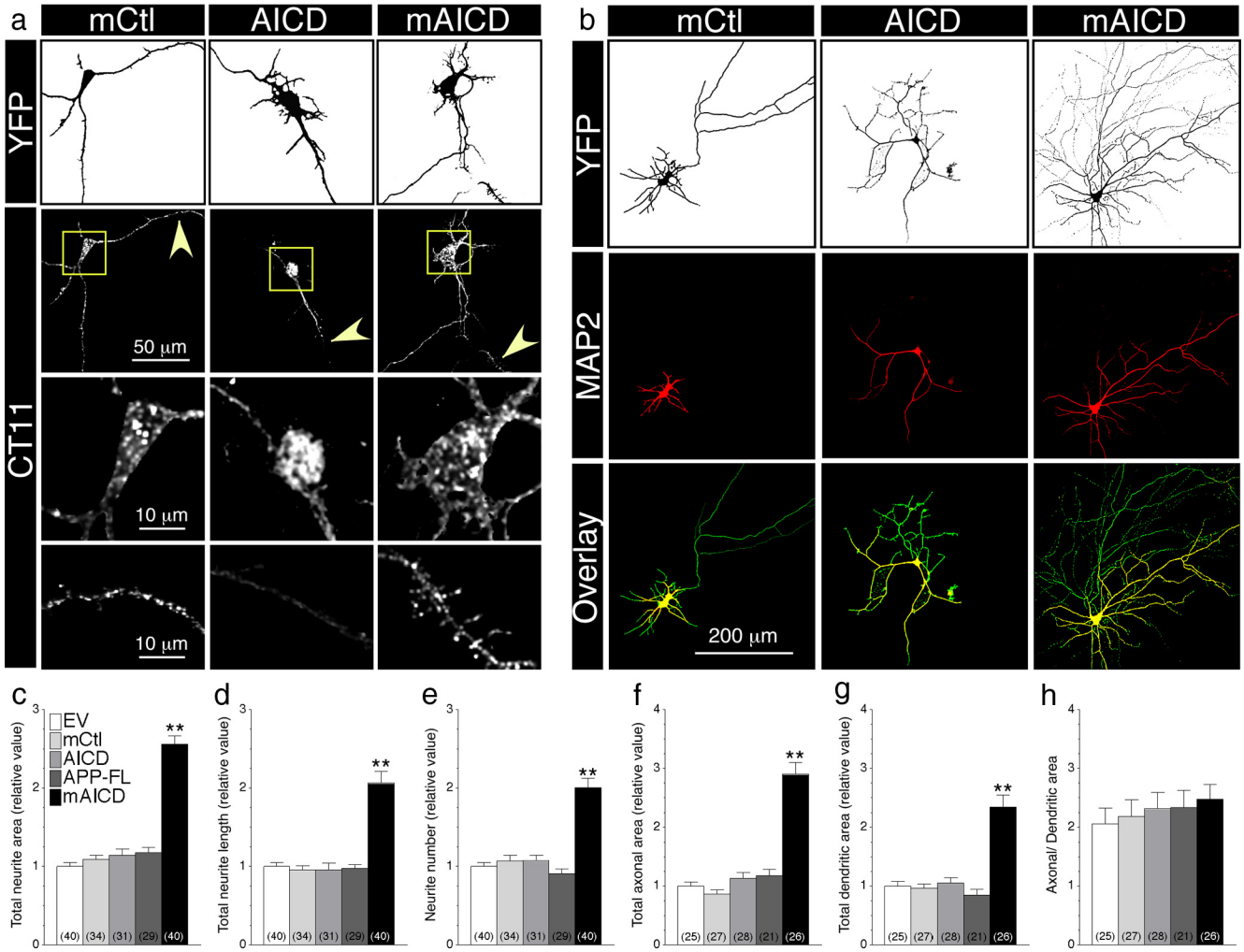


**Figure 2.** Membrane-tethered APP intracellular domain promotes exuberant axonal and dendritic arborization in mouse cortical neurons. ***a***, Distribution of mCtl, AICD, and mAICD in primary cortical neurons (8–14 DIV) cotransfected with YFP and the indicated plasmids and immunostained with CT11 antibody. *Z*-stack images (200 nm interval) were deconvolved and processed for quantification. YFP fluorescence is depicted as inverted images. The bottom two panels represent CT11 staining in enlarged somatic (boxed region) and dendritic areas (indicated by arrowheads). ***b***, Neurons were transfected as above and immunostained with MAP2 antibody. YFP fluorescence is shown as inverted image, and MAP2 staining is shown in red. Overlay images (bottom panel) reveal axons (green) and dendrites (yellow). ***c–h***, Quantitative analysis of neurite outgrowth. Total neurite area (***c***), total neurite length (***d***), and neurite number (***e***) in primary cortical neurons expressing various constructs are plotted relative to YFP/EV-transfected neurons. Total axonal (***f***) and dendritic areas (***g***) were also quantified in the same groups of neurons. Differences in axonal and dendritic networks are shown as a change in the ratio between both areas (***h***). Statistical analysis was performed using ANOVA Kruskal–Wallis test followed by Dunn's *post hoc* multiple-comparison analysis. $^{**}p < 0.001$, compared with neurons transfected with an EV control. The total number of quantified neurons is shown in parentheses. Error bars indicate SEM.

and mounted using Permafluor mounting medium (Thermo Fisher Scientific).

*Image acquisition, processing, and analysis.* Labeled neurons were imaged using a motorized Nikon TE 2000 microscope and Cascade II:512 CCD camera (Photometrics) using 20×, 60× (NA 1.49) or 100× (NA 1.45) objectives. Images were acquired as 200 nm *z*-stacks and processed using MetaMorph software (Molecular Devices). For visualization and analysis of colocalization, deconvolved *z*-stack images were generated using Huygens software (Scientific Volume Imaging). NeuronJ plug-in (version 1.29) of ImageJ software was used to measure neurite number and length of cortical neurons (Abramoff et al., 2004; Deyts et al., 2009). Total neurite length was evaluated by manually tracing all neurites in each neuron. In neurons, total neurite area was evaluated using thresholding feature of MetaMorph software to isolate the cell of interest, followed by somatic area removal from YFP-expressing cells. Similarly, total neurite area was evaluated in H19-7 and N2a cells through image subtraction of a predefined somatic area applied to each cells. Total axonal area was determined by subtraction of total dendritic area (as seen as MAP2 labeling) from total neurite area (as seen as YFP fluorescence). To quantify the level of fluorescence, identical parameters and photomultiplicator values were used to acquire the images. Raw images were first set to the same threshold level to eliminate nonspecific fluorescence, and then the gray intensity level was determined and divided by the number of pixels per area (calculated from YFP fluorescence image). Colocalization was evaluated by the degree of fluorescence-overlapping area between two fluorophores using Pearson's coefficient analysis from JACoP plug-in of ImageJ.

*Statistical analysis.* Each experiment was performed using at least three independent sets of cultures. Data are presented as mean ± SEM. Statistical significance was determined by ANOVA Kruskal–Wallis test with independent *post hoc* Dunn's multiple-comparison analysis using GraphPad prism software. $^{*}p < 0.05$, $^{**}p < 0.001$, compared with EV-transfected cells, and $^{\#}p < 0.05$ and $^{\#\#}p < 0.001$, compared with untreated cells within the same transfected conditions.

## Results

### Accumulation of membrane-bound APP intracellular domain enhances neurite outgrowth in N2a cells

Proteolytic processing of APP-FL by $\alpha$- and $\beta$-secretases generates membrane-bound APP-CTFs, which preferentially localize to lipid raft microdomains in cultured cell lines and in the brain

(for review, see Cheng et al., 2007). These CTFs are subsequently cleaved by γ-secretase at the γ- and ε-sites, to release Aβ and AICD, respectively, from the membrane (for review, see Thinakaran and Koo, 2008; Lichtenthaler et al., 2011). To investigate intracellular signaling mediated by APP and APP-CTF at the membrane, we generated a fusion protein, termed mAICD, in which the extracellular and transmembrane domains of human APP were replaced by 17 residues corresponding to the N-terminal myristoylation and palmitoylation (MyrPalm) motif of the Src family tyrosine kinase Lyn (Fig. 1*a*) (Zacharias et al., 2002). Fractionation of transfected mouse N2a neuroblastoma cells revealed membrane association of mAICD and a 47 aa control polypeptide with an N-terminal MyrPalm motif (mCtl) as expected, and confirmed the presence of AICD in the nuclear fraction (Fig. 1*b*). Sucrose density gradient fractionation analysis further revealed predominant membrane raft association of mAICD (Fig. 1*c*), which faithfully mimics preferential raft localization of APP-CTFs derived from processing of APP-FL in cultured cell lines and in mouse brain (Vetrivel et al., 2005). Thus, subcellular localization studies establish that mAICD is retained at the membrane, especially in membrane microdomains. Membrane microdomains are known to compartmentalize numerous membrane-associated receptor-activated signaling cascades, including neurotransmitter signaling (Allen et al., 2007). Consistent with the recruitment of signaling molecules, expression of mAICD in N2a cells significantly increased total neurite area compared with EV control. However, expression of APP-FL, AICD, or membrane-tethered mCtl did not affect the level of neurite outgrowth (Fig. 1*e*,*f*).

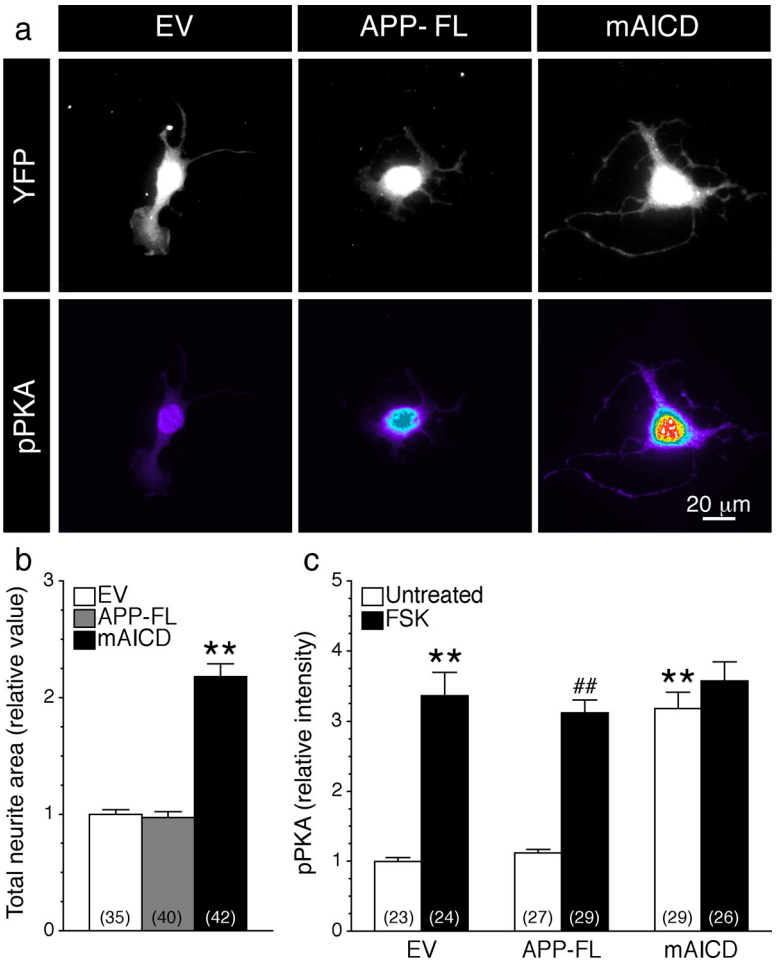


**Figure 3.** Accumulation of membrane-tethered APP intracellular domain-induced neurite outgrowth parallels phosphorylation of PKA substrates in hippocampal H19-7 cells. ***a***, H19-7 cells cotransfected with YFP and EV, APP-FL, or mAICD were allowed to differentiate for 24 h and immunostained with an antibody directed against phosphorylated Ser/Thr PKA substrates (pPKA) (Grønborg et al., 2002). Images of YFP fluorescence are shown in gray, whereas intensity of pPKA staining is shown in pseudocolor. ***b***, Total neurite area was quantified as described in Materials and Methods and plotted relative to EV-transfected cells. ***c***, The intensity of pPKA staining was quantified and plotted relative to the signal intensity in EV-transfected cells. The black bars represent the signal in cells treated with FSK (50 μM; 30 min). Statistical analysis was performed using ANOVA Kruskal–Wallis test followed by Dunn's *post hoc* multiple-comparison analysis. $^{**}p < 0.001$, compared with EV untreated cells, and $^{\#\#}p < 0.001$, compared with untreated cells within the same transfected conditions. The total number of quantified cells is shown in parentheses. Error bars indicate SEM.

To examine whether CTFs generated by processing of APP-FL by α- and β-secretases also stimulate neurite outgrowth, we incubated cells with the γ-secretase inhibitor Compound E (Seiffert et al., 2000), which produced an accumulation of APP-CTFs in cells transfected with APP-FL (Fig. 1*d*). This accumulation of APP-CTFs caused a marked increase of neurite extension (Fig. 1*e*,*f*). As expected, treatment with Compound E did not have noticeable effect on the steady-state levels of mCtl, AICD, or mAICD. Expression of mCtl and AICD did not affect N2a cell morphology, and the treatment with Compound E had no additional influence of neurite outgrowth in cells expressing mAICD (Fig. 1*e*,*f*). Thus, enhanced neurite outgrowth in these experiments is entirely attributed to membrane accumulation of APP-CTF.

We evaluated the linear relationship between the level of mAICD expression and the total cellular area. As shown in Figure 1*g*, increase of N2a area correlate significantly with the level of mAICD expression, either revealed by cotransfected YFP fluorescence ( $y = 0.887x + 0.678$; $r^2 = 0.560$; $p < 0.001$) or immunostaining of tagged mAICD polypeptide ( $y = 0.939x + 0.709$; $r^2 = 0.626$; $p < 0.001$). Expression levels of YFP alone did not show any significant correlation with cellular area ( $y = 0.015x + 0.972$; $r^2 = 0.001$; $p = 0.899$). Together, our results support the idea that accumulation of membrane-tethered APP-CTF, either by inhibiting the γ-secretase-dependent processing of APP-CTF or by targeting APP intracellular domain to the membrane using the motifs that direct myristylation/palmitoylation, influences neurite formation.

### Membrane-tethered APP intracellular domain promotes exuberant axonal and dendritic arborization in mouse cortical neurons

Next, we assessed whether membrane accumulation of APP intracellular domain affects neurite extension in primary mouse cortical neurons. We observed that MyrPalm motif containing polypeptides (mAICD and mCtl) localized to punctate membranous structures in the cell body as well as dendrites and axons, whereas AICD expression was mainly found in the nucleus and within larger caliber primary dendrites (Fig. 2*a*). As in N2a cells,

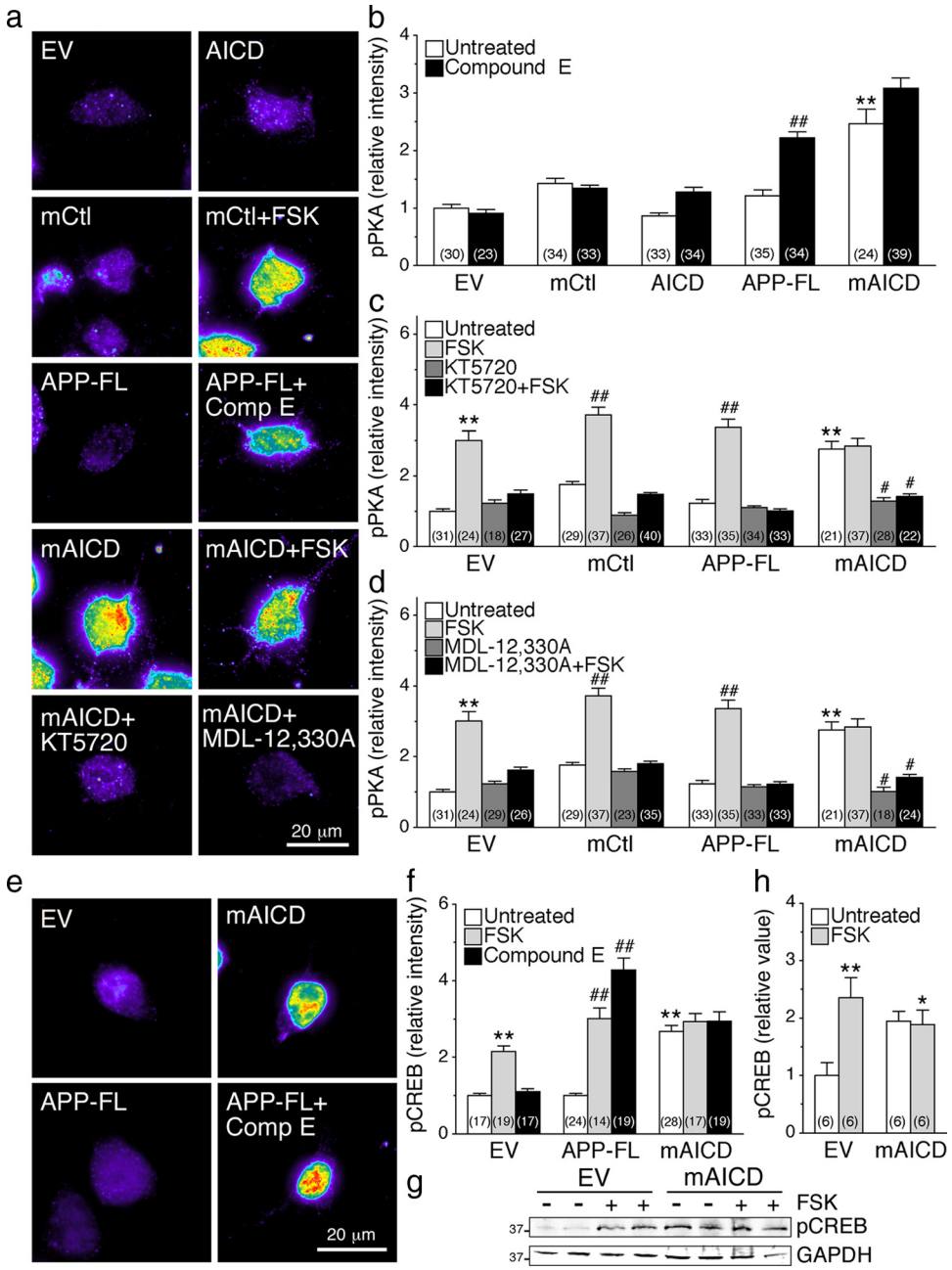


**Figure 4.** Activation of cAMP/PKA pathway in N2a cells expressing membrane-tethered APP intracellular domain. N2a cells cotransfected with YFP and EV, mCtl, AICD, APP-FL, or mAICD were immunostained with phosphorylated Ser/Thr PKA substrate antibody (pPKA) (Grønborg et al., 2002) or phosphorylated (Ser [133]) CREB antibody (pCREB) (Ginty et al., 1993). ***a***, Representative pseudocolor images of pPKA immunofluorescence staining intensity in treated or untreated cells expressing various constructs. ***b–d***, Quantitative analysis of pPKA staining intensity. Changes in pPKA staining intensity following treatment with Compound E (10 nM; 24 h) (***b***), adenylate cyclase activator FSK (50 $\mu$M; 30 min) and PKA inhibitor KT5720 (2 $\mu$M; 30 min) (***c***), and adenylate cyclase inhibitor MDL-12,330A (10 nM; 30 min) (***d***) were plotted. ***e***, Representative pseudocolor images of pCREB immunofluorescence in cells expressing EV, mAICD, or APP-FL. ***f***, Changes in the levels of pCREB staining intensity under basal conditions and after treatment with FSK or Compound E are plotted. ***g***, Representative Western blot of pCREB in stable N2a cells expressing EV or mAICD without or after FSK stimulation (50 $\mu$M; 30 min) is shown. GAPDH was used for loading control. ***h***, Quantitative analysis is shown as relative change in the ratio of pCREB intensity over intensity of EV control. Statistical analysis was performed using ANOVA Kruskal–Wallis test followed by Dunn's *post hoc* multiple-comparison analysis. $^{*}p < 0.05$, $^{**}p < 0.001$, compared with untreated EV-transfected cells; and $^{\#}p < 0.05$, $^{\#\#}p < 0.001$, compared with untreated cells within the same transfected conditions. The total number of quantified cells is shown in parentheses. Error bars indicate SEM.

expression of mAICD in pyramidal neurons significantly increased total neurite area compared with EV or mCtl (Fig. 2*b*,*c*). Notably, expression of APP-FL and AICD did not affect the level of neurite outgrowth. Expression of mAICD caused a twofold increase of the total neurite length (Fig. 2*d*; $p < 0.001$) as well as neurite number per branches (Fig. 2*e*; $p < 0.001$). Further analysis revealed that mAICD expression increased both the axonal and dendritic network (Fig. 2*f*,*g*, respectively) without an apparent bias toward either neuronal compartment (Fig. 2*h*). Together, these results provide the first evidence that membrane-tethered APP cytosolic domain affects neurite outgrowth in cultured neurons.

### mAICD-induced neurite outgrowth parallels increased phosphorylation of PKA substrates in hippocampal H19-7 cells

To investigate the signaling events associated with mAICD-induced neurite outgrowth, we used immortalized hippocampal

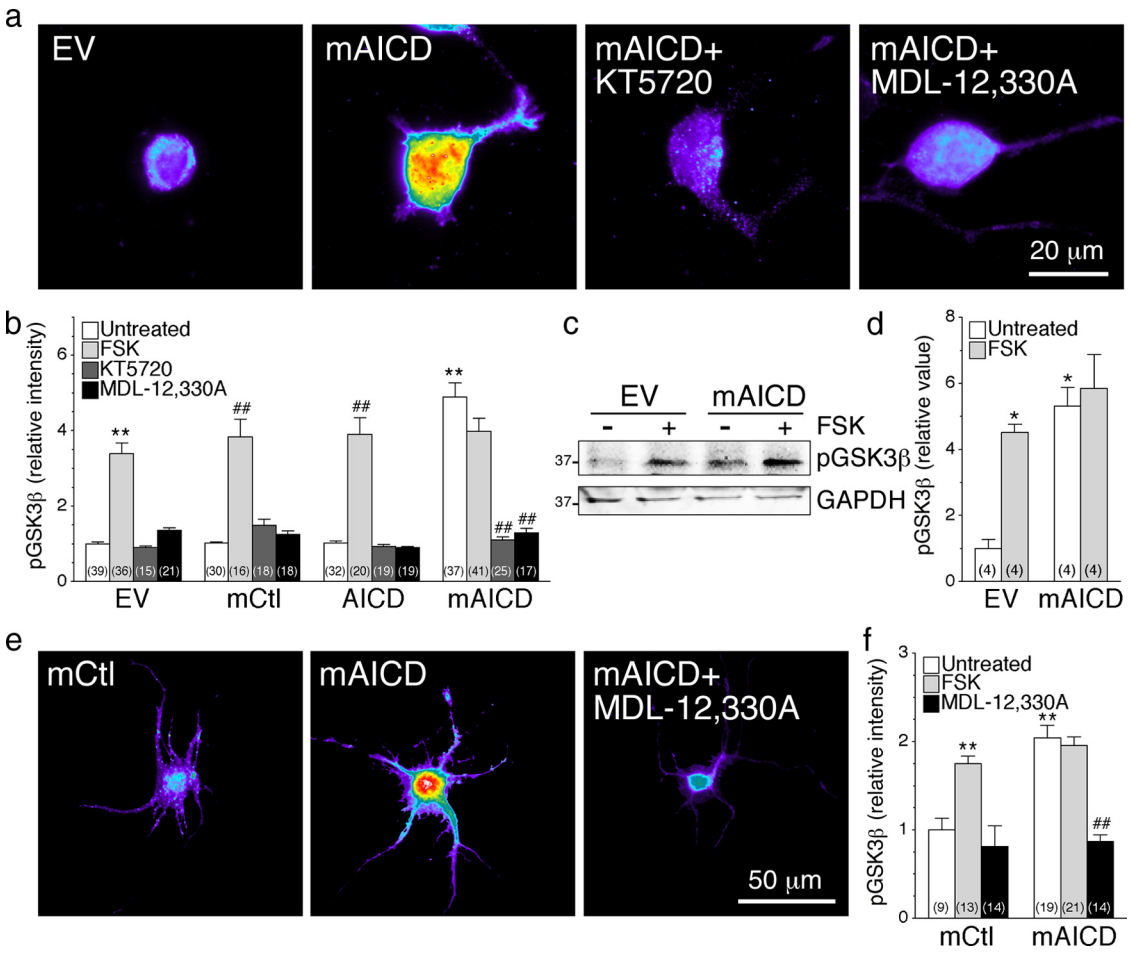


**Figure 5.** cAMP/PKA-dependent inhibition of GSK3$\beta$ pathway in cells expressing membrane-tethered APP intracellular domain. N2a cells coexpressing YFP and EV, mCtl, AICD, or mAICD were immunostained with antibodies directed against phosphorylated (Ser$^9$) GSK3$\beta$ (pGSK3$\beta$). CCD images were acquired (100× objective) and processed by applying a common threshold between groups using MetaMorph software. Representative pseudocolor images of N2a cells (***a***) and cortical neurons (***e***) show pGSK3$\beta$ staining intensity in treated or untreated cells expressing various constructs. ***b***, ***f***, Quantitative analysis of pGSK3$\beta$ staining intensity is represented as relative changes compared with EV or mCtl basal level. Changes in intensity levels are shown after FSK stimulation (50 $\mu$M; 30 min) before and after treatment with PKA (KT5720; 2 $\mu$M, 1 h) or adenylate cyclase (MDL-12,330A; 10 nM, 1 h) inhibitors. ***c***, Representative Western blot of pGSK3$\beta$ in stable N2a cells expressing EV or mAICD under basal conditions and after treatment with FSK. GAPDH was used for loading control. ***d***, Quantitative analysis is shown as relative change in the ratio of pGSK3$\beta$ intensity over intensity of EV control. Statistical analysis was performed using ANOVA Kruskal–Wallis test followed by Dunn's *post hoc* multiple-comparison analysis for immunostaining and Tukey's multiple-comparison test for Western blots. $^*p < 0.05$, $^{**}p < 0.001$, compared with untreated EV-expressing cells; and $^{\#\#}p < 0.001$, compared with untreated cells within the same transfected conditions. Total number of N2a cells (from at least 3 independent sets of cultures) used for quantification is shown in parentheses. Error bars indicate SEM.

H19-7 cell line, which exhibits neuronal phenotype, conditional proliferation, and a capacity for differentiation after cessation of division (Eves et al., 1992; Wu et al., 2004) (Fig. 3). As we observed in primary neurons and N2a neuroblastoma cells, expression of mAICD stimulated neurite extension in hippocampal H19-7 cells (Fig. 3*a*, top panel). Quantitative analysis of total neurite area using YFP fluorescence, revealed that neurite outgrowth was more than twofold increased in mAICD-expressing cells, whereas expression of APP-FL had no effect over vector control (Fig. 3*b*).

We tested whether mAICD expression leads to activation of cAMP/PKA signaling because basic neuronal morphology as well as initial steps in neuronal elongation could be dependent on the activation of cAMP/PKA pathway (Sanchez et al., 2001; Hutchins, 2010; Shelly et al., 2010). When transfected cells were immunostained with an antibody that specifically recognizes substrates phosphorylated by PKA (pPKA substrates; characterized by Arg at position −3 relative to the phosphorylated Ser or Thr) (Grønborg et al., 2002; Barnes et al., 2008), we observed a significant increase of pPKA substrate staining intensity in cells expressing mAICD relative to cells transfected with EV- and APP-FL-expressing cells (Fig. 3*a*, bottom panel; *c*; EV, 1.00 ± 0.05; APP-FL, 1.12 ± 0.05; mAICD, 3.18 ± 0.23; $p < 0.001$). Following treatment with FSK, an adenylate cyclase activator, the intensity of pPKA substrates staining in EV and APP-FL markedly increased by more than threefold, while no further increase was observed in mAICD-expressing cells (Fig. 3*c*).

### Activation of cAMP/PKA pathway in N2a cells expressing membrane-tethered APP intracellular domain

To examine putative signaling pathways associated with accumulation of membrane-bound APP-CTF and enhanced neurite outgrowth, we also immunostained N2a cells with Ser/Thr pPKA antibody. As observed in H19-7 cells, expression of mAICD resulted in enhanced phosphorylation of PKA substrates in N2a cells (Fig. 4*a*,*b*). When APP-FL-expressing cells were incubated with Compound E, a treatment that caused accumulation of APP-CTF and increase of neurite outgrowth, the intensity of pPKA substrate staining also increased by more than twofold (Fig. 4*b*; $p < 0.001$). However, as expected from the lack of neurite out-

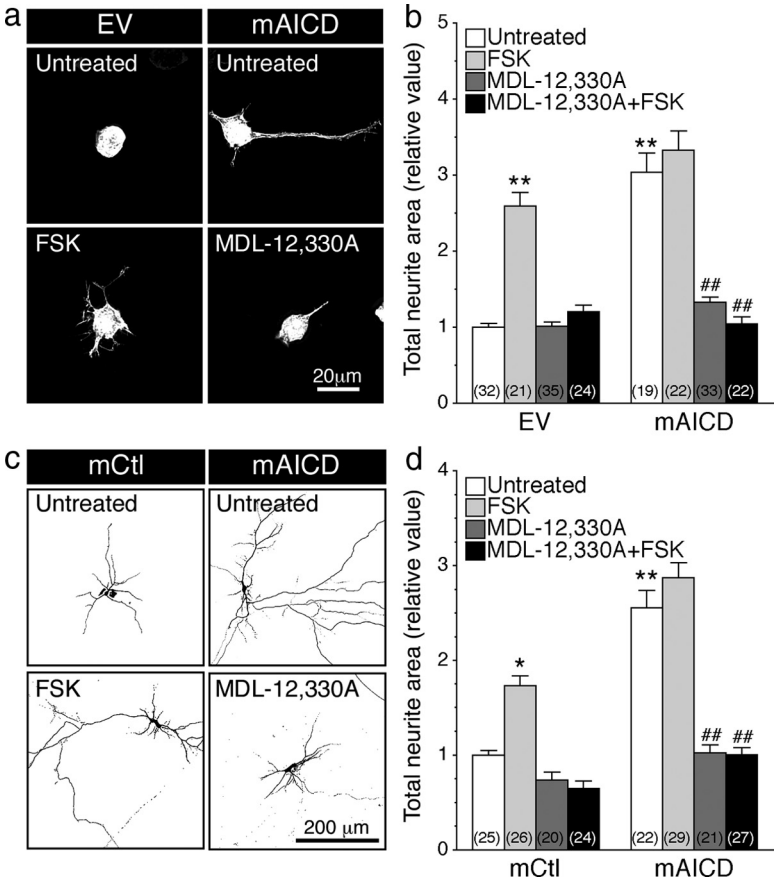


**Figure 6.** Accumulation of membrane-tethered APP intracellular domain-induced neurite outgrowth requires adenylate cyclase activation. N2a cells and cortical neurons coexpressing YFP and EV, mCtl, or mAICD were stimulated with FSK (1 $\mu$M; 24 h) and/or treated with adenylate cyclase inhibitor MDL-12,330A (10 nM; 24 h), and neurite extensions were quantified as described in Materials and Methods. Representative images of N2a cells (***a***) or inverted images of cortical neurons (***c***) are shown. ***b***, ***d***, Three-dimensional deconvolved images were quantified, and morphological changes following FSK stimulation and/or application of adenylate cyclase inhibitor MDL-12,330A (10 nM; 24 h) are plotted as relative difference of total neurite area compared with untreated EV or mCtl controls. Statistical analysis was performed using ANOVA Kruskal–Wallis test followed by Dunn's *post hoc* multiple-comparison analysis. $^{*}p < 0.05$, $^{**}p < 0.001$, compared with untreated EV- or mCtl-expressing cells; $^{\#\#}p < 0.001$, compared with untreated cells within the same transfected conditions. The total number of quantified cells is shown in parentheses. Error bars indicate SEM.

growth (outlined above), Compound E treatment failed to affect PKA-dependent signaling in mCtl or cells expressing AICD. Furthermore, treatment with Compound E did not significantly show any additive effect in the level of pPKA substrate intensity in mAICD-expressing cells compared with untreated cells, which is in agreement with the neurite outgrowth data.

To establish the involvement of cAMP/PKA signaling in the observed increase of pPKA substrate staining intensity in mAICD-expressing cells, we used pharmacological inhibition of PKA and adenylate cyclase. As shown in Figure 4*c*, we observed that acute incubation with KT5720, a specific PKA inhibitor, abolished the cAMP-dependent increase of pPKA staining in FSK-treated cells transfected with EV, mCtl, or APP-FL. Similarly, incubation with MDL-12,330A, a specific adenylate cyclase inhibitor, also abrogated FSK-mediated increase of pPKA staining (Fig. 4*d*). More interestingly, mAICD expression-related increase of pPKA staining was also abolished by incubation with either KT5720 (Fig. 4*c*; $p < 0.05$) or MDL-12,330A (Fig. 4*d*; $p < 0.05$).

We also quantified the levels of phosphorylated cAMP response element-binding protein-1 (pCREB), which is one of the key neuronal targets of activated PKA and axonal outgrowth (Lonze and Ginty, 2002). At steady state, we observed higher levels of pCREB staining in N2a cells expressing mAICD compared with those expressing APP-FL or the EV control (Fig. 4*e*,*f*; $p < 0.001$). Following acute stimulation with FSK, the intensity of pCREB staining was enhanced in EV- and APP-FL-expressing cells (Fig. 4*f*). No further increase in pCREB staining was found in mAICD-expressing cells following FSK stimulation. Consistent with the involvement of membrane-bound APP-CTFs in activating PKA-dependent signaling, treatment with Compound E increased pCREB levels by more than fourfold in cells expressing APP-FL (Fig. 4*f*; $p < 0.001$), an effect that was not observed in EV- or mAICD-expressing cells. Western blot analysis confirmed that levels of pCREB are increased by approximately twofold in FSK-treated cells as well as in cells stably expressing mAICD compared with EV (Fig. 4*g*,*h*). As seen by immunostaining, we observed no further increase of pCREB in FSK-treated mAICD cells (Fig. 4*h*). Collectively, these results confirm the involvement of pPKA substrates in the sequence of events leading up to enhanced neurite outgrowth following mAICD expression or the accumulation of membrane-tethered APP-CTF generated from processing of APP-FL.

### cAMP/PKA-dependent inhibition of GSK3$\beta$ pathway in N2a cells expressing membrane-tethered APP intracellular domain

It has been shown that activation of cAMP/PKA and GSK3$\beta$ signaling pathways are both necessary for the initial elongation of neurites in neuronal cell types (Sanchez et al., 2001; Hutchins, 2010). Interestingly, $Ser^{9}$ in GSK3$\beta$ is a physiological substrate of PKA, and phosphorylation at this residue leads to inactivation of GSK3$\beta$ (Fang et al., 2000; Jope and Johnson, 2004; Shelly et al., 2010). Since GSK3$\beta$ activation is associated with neurite retraction, and inhibition of GSK3$\beta$ promotes axonal elongation (Yoshimura et al., 2006; Hur and Zhou, 2010; Shelly et al., 2010), we considered the possibility that neurite outgrowth stimulated by expression of membrane-tethered APP-CTF might involve a cross talk between PKA and GSK3$\beta$ signaling cascades. To assess GSK3$\beta$ activity in individual cells, we stained transfected N2a cells and cultured cortical neurons using an antibody that recognizes inactive $Ser^{9}$ phosphorylated GSK3$\beta$ (pGSK3$\beta$). Overexpression of mAICD caused a twofold to fivefold increase in pGSK3$\beta$ levels in the soma and neurites of pyramidal neurons and N2a neuroblastoma cells, respectively, whereas expression of AICD had no effect (Fig. 5). FSK-induced activation of cAMP/PKA was also associated with an increase of pGSK3$\beta$ fluorescence intensity in mCtl- and AICD-expressing cells consistent with previous reports (Fang et al., 2000; Jope and Johnson, 2004; Shelly et al., 2010), but there was no further increase in cells expressing mAICD (Fig. 5*b*,*d*). More importantly, PKA inhibitor (KT5720) and adenylate cyclase inhibitor (MDL-

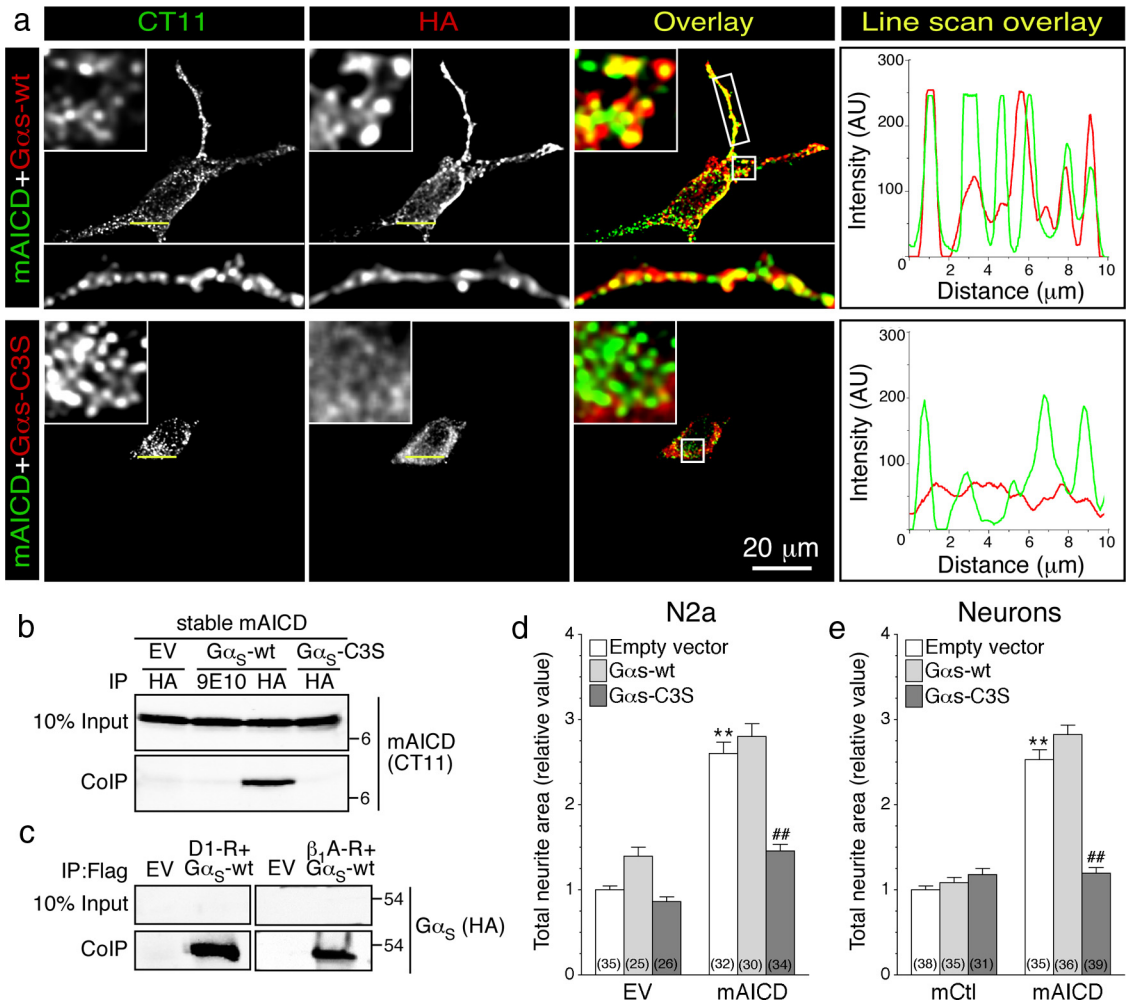


**Figure 7.** Functional coupling of membrane-tethered APP intracellular domain with $G\alpha_s$-protein. ***a***, Immunofluorescence localization of mAICD and HA-tagged wild-type $G\alpha_s$ ($G\alpha_s$-wt) or dominant-negative $G\alpha_s$ mutant ($G\alpha_s$-C3S) in N2a cells. The boxed regions are shown as enlarged insets. Line scans (right panels) show overlapping peaks of mAICD (green) and $G\alpha_s$-wt (red) localization along a small stretch in the cell body. ***b***, Coimmunoprecipitation analysis of mAICD interaction with $G\alpha_s$ was evaluated in stable N2a cells expressing mAICD following transient transfection of $G\alpha_s$-wt. Non-denaturing lysates were immunoprecipitated with mAb HA or mAb 9E10 (negative control) and analyzed by immunoblotting with CT11 to detect mAICD. ***c***, As positive control, interaction between dopamine $D_1$ receptor (D1-R) or $\beta 1$ adrenergic receptor ($\beta_1$A-R) and $G\alpha_s$-wt was analyzed by coimmunoprecipitation. ***d***, ***e***, Quantification of neurite outgrowth in N2a cells (***d***) or cortical neurons (***e***) 24 h following cotransfection of EV, mCtl, or mAICD with $G\alpha_s$-Wt or $G\alpha_s$-C3S. Statistical significance was examined by ANOVA Kruskal–Wallis test followed by Dunn's *post hoc* multiple-comparison analysis. $^{**}p < 0.001$, compared with EV/EV or EV/mCtl control cells. $^{\#\#}p < 0.001$, compared with EV within mAICD transfected group when cells are G-protein transfected. The total number of quantified cells is shown in parentheses. Error bars indicate SEM.

12,330A) completely abolished mAICD-induced increase in pGSK3$\beta$ levels in N2a cells (Fig. 5*a*,*b*; untreated, 4.89 ± 0.37; KT5720, 1.16 ± 0.07; MDL-12,300A, 1.15 ± 0.09), as well as in cortical neurons (Fig. 5*e*,*f*; untreated, 1.98 ± 0.03; MDL-12,300A, 1.05 ± 0.08). Consistent with the immunofluorescence results, Western blot analysis of stably transduced N2a pools confirmed that the basal levels of pGSK3$\beta$ were approximately fivefold higher in stable mAICD pools compared with the EV cells (Fig. 5*c*,*d*). Furthermore, treatment with FSK induced phosphorylation of GSK3$\beta$ by more than fourfold in EV cells, whereas there was no further increase in cells stably expressing mAICD. Together, our results support the idea that targeting APP intracellular domain at the membrane is closely associated with GSK3$\beta$ inactivation through adenylate cyclase/PKA cascade. Since inhibition of GSK3$\beta$ promotes axon outgrowth (Yoshimura et al., 2006; Hur and Zhou, 2010), these results indicate that control of GSK3$\beta$ activity via $Ser^9$ phosphorylation might also contribute to the increase of neurite formation seen in mAICD-expressing cells.

### Membrane-tethered APP intracellular domain-induced neurite outgrowth requires adenylate cyclase activation

Based on the results detailed above, we predicted that accumulation of membrane-tethered APP-CTF or expression of mAICD is associated with activation of adenylate cyclase signaling cascade, which could be required for neurite outgrowth. Accordingly, we investigated the requirement of adenylate cyclase for neurite outgrowth associated with membrane-bound APP-CTFs in N2a cells and cortical neurons by treating cells for 24 h with an adenylate cyclase activator (FSK) or the inhibitor (MDL-12,330A). As expected from previous reports (Sanchez et al., 2001; Hutchins, 2010; Shelly et al., 2010), chronic activation of cAMP pathway enhanced neurite outgrowth in control N2a cells (Fig. 6*a*,*b*) and cortical neurons (Fig. 6*c*,*d*). However, treatment with FSK did not show any additive effect in cells expressing mAICD (Fig. 6*b*,*d*), suggesting that mAICD expression acts upstream of adenylate cyclase activation and that cAMP-dependent signaling might have reached maximal physiological outcome. As expected, treatment with the adenylate cyclase inhibitor MDL-

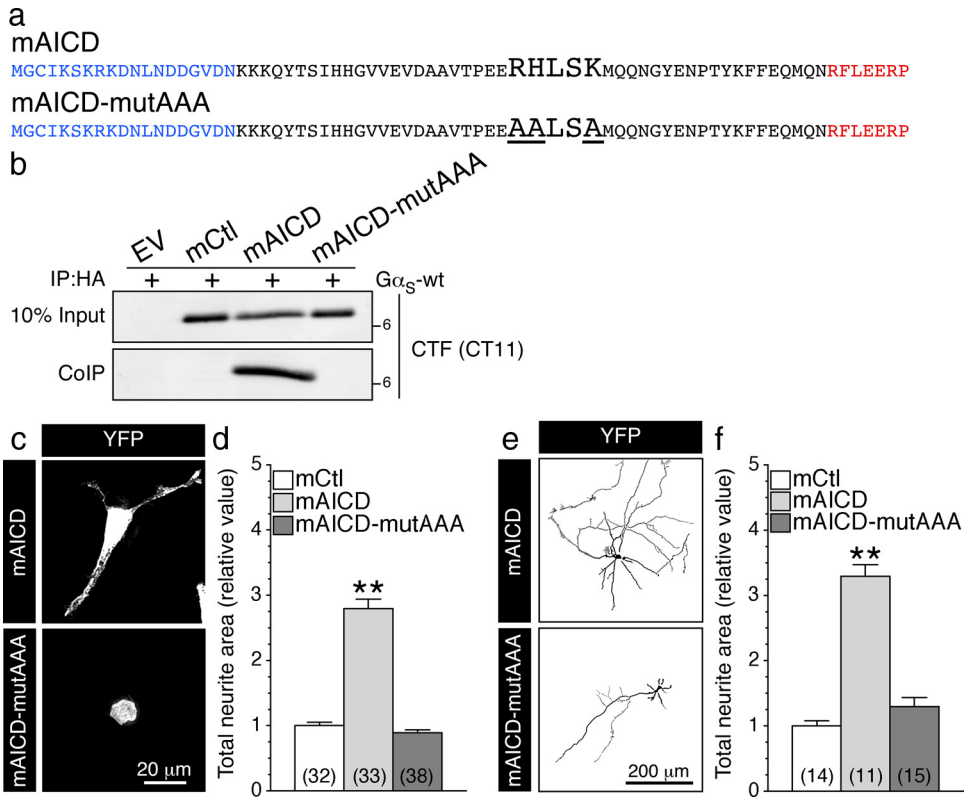


**Figure 8.** APP intracellular domain BBXXB motif is required for interaction with Gα$_S$ and mAICD-induced neurite outgrowth. ***a***, The amino acid sequences of mAICD constructs are shown. The "BBXXB" motif RHLSK was mutated to AALSA to generate mAICD-mutAAA. ***b***, Coimmunoprecipitation analysis of mAICD and mAICD-mutAAA with Gα$_S$ in transfected N2a cells. Note that the BBXXB motif is essential for mAICD interaction with Gα$_S$. ***c***, ***e***, Representative images of N2a cells (***c***) and 8 DIV cortical neurons (***e***) coexpressing YFP and mAICD or mAICD-mutAAA. ***d***, ***f***, Analysis of the morphological changes in cells (or neurons) transfected with mAICD or mAICD-mutAAA were quantified from 3-D deconvolved image stacks that are plotted relative to cells (or neurons) transfected with mCtl. Statistical analysis was performed using ANOVA Kruskal–Wallis test followed by Dunn's *post hoc* multiple-comparison analysis. $^{**}p < 0.001$, compared with mCtl-expressing N2a cells or cortical neurons. The total number of quantified cells is shown in parentheses. Error bars indicate SEM.

12,330A eliminated FSK-induced neurite extension in EV-transfected N2a cells and neurons (Fig. 6*b*,*d*, respectively). More importantly, mAICD expression-induced neurite extension was abolished following MDL-12,330A treatment in N2a cells (Fig. 6*a*, bottom right; *b*; untreated, 3.04 ± 0.26; MDL-12,330A, 1.05 ± 0.09; $p < 0.001$) and in cortical neurons (Fig. 6*c*, bottom right, *d*; untreated, 2.56 ± 0.18; MDL-12,330A, 1.00 ± 0.07; $p < 0.001$). Together, these results indicate that mAICD-induced neurite outgrowth takes place downstream of adenylate cyclase activation. Therefore, it becomes apparent that activation of adenylate cyclase is necessary and sufficient to initiate morphological changes associated with membrane accumulation of APP intracellular domain.

### Functional coupling of membrane-tethered APP intracellular domain with Gα$_S$-protein

Next, to characterize adenylate cyclase-associated signaling molecule(s) that function downstream of APP-CTF, we focused our attention on guanine nucleotide-binding protein G(s) subunit α (Gα$_S$), the canonical signal transducer that links receptor-ligand interactions with the activation of adenylyl cyclase. In stably transfected N2a cells, mAICD localized to cellular membranes as clusters. Transiently expressed wild-type Gα$_S$ (Gα$_S$-wt) also localized as clusters on the plasma membrane and other organelles, and strongly overlapped with mAICD, especially in neurite extensions (Fig. 7*a*). Interestingly, a dominant-negative Gα$_S$ mutant that could not be palmitoylated (Gα$_S$-C3S) showed poor colocalization with mAICD as visualized by line scan histogram (Fig. 7*a*). Pearson's correlation coefficient analysis confirmed greater colocalization of mAICD with Gα$_S$-wt compared with Gα$_S$-C3S mutant (Gα$_S$-wt, 0.591 ± 0.030; Gα$_S$-C3S, 0.369 ± 0.047; $p < 0.01$). In agreement with these findings, mAICD efficiently coimmunoprecipitated with Gα$_S$ from non-denaturing lysates of transfected N2a cells (Fig. 7*b*), under conditions that preserved the interaction of Gα$_S$ with $D_1$-dopamine and β1-adrenergic receptors, two canonical receptors that signal through Gα$_S$ (Fig. 7*c*). Consistent with poor colocalization, Gα$_S$-C3S mutant failed to coimmunoprecipitate with mAICD (Fig. 7*b*). Finally, analysis of neurite outgrowth revealed that coexpression of Gα$_S$-wt had no effect, whereas expression of the dominant-negative Gα$_S$-C3S mutant significantly inhibited mAICD-induced neurite extension in N2a cells (Fig. 7*d*; mAICD plus Gα$_S$-wt, 2.80 ± 0.15; mAICD plus Gα$_S$-C3S, 1.46 ± 0.08; $p < 0.001$) and in primary neurons: (Fig. 7*e*; mAICD plus Gα$_S$-wt, 2.82 ± 0.11; mAICD plus Gα$_S$-C3S, 1.20 ± 0.07; $p < 0.001$). Together, these findings indicate that Gα$_S$-protein coupling is an essential part of the signaling pathway that translates mAICD expression to promote neurite outgrowth.

### APP C-terminal domain interaction with BBXXB motif is required for neurite outgrowth

To further establish a direct link between APP C-terminal domain and Gα$_S$-protein, we scanned the amino acid sequence of APP intracellular domain for the presence of specific motifs such as BBXXB, BXBXB, BBXB, BXBB, or BXB (where B represents a basic amino acid residue and X represents a nonbasic residue), which have been identified as G-protein binding sites within the

intracellular domains of G-protein-coupled receptors (Okamoto et al., 1990; Wu et al., 1995; Pauwels et al., 1999; Zhou and Murthy, 2003). APP intracellular domain possesses a single highly conserved BBXXB motif: $^{672}$RHLSK$^{676}$ ($APP_{695}$ isoform numbering). To test the possibility that RHLSK sequence on APP C-terminal domain is the critical site of interaction with $G\alpha_S$ subunit, we introduced alanine substitution of the basic residues in mAICD to convert the BBXXB motif to **AA**LS**A** (named mAICD-mutAAA; Fig. 8*a*). Coimmunoprecipitation experiments confirmed lack of interaction between $G\alpha_S$ and mAICD-mutAAA (Fig. 8*b*). Consistent with its inability to associate with $G\alpha_S$, expression of mAICD-mutAAA had no effect on neurite extension in N2a cells (Fig. 8*c*,*d*) and cortical neurons (Fig. 8*e*,*f*). These results clearly establish that APP-CTF possesses a sequence motif for interaction with $G\alpha_S$, and functional coupling with $G\alpha_S$ transduces signaling downstream of mAICD expression to induce neurite outgrowth.

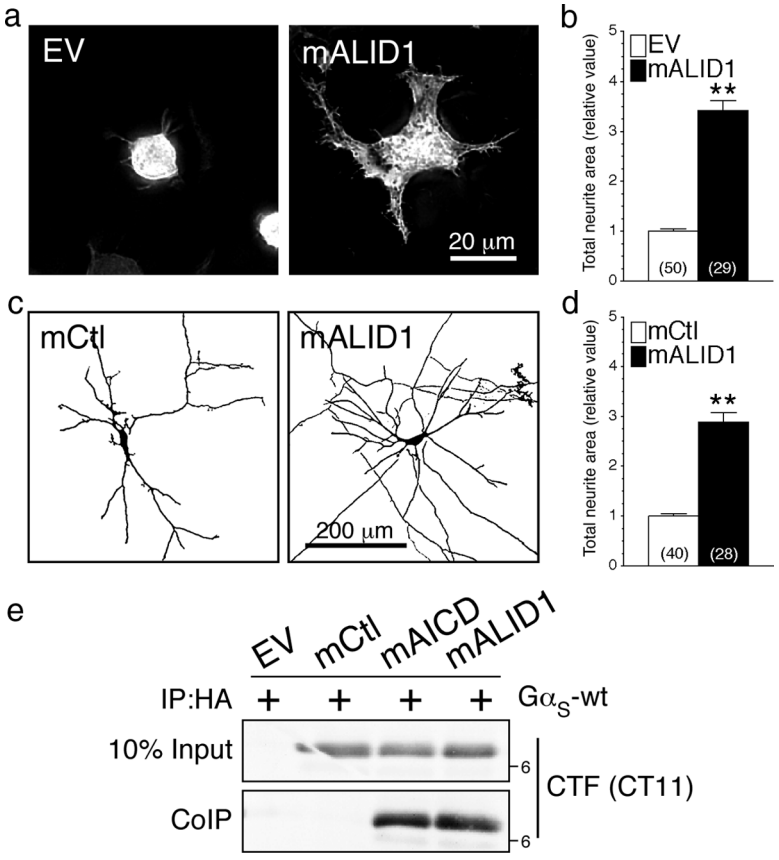


**Figure 9.** Functional coupling of membrane-targeted APLP1 homolog with $G\alpha_S$-protein. N2a cells and cortical neurons were cotransfected with YFP and EV or mALID1. Representative images of N2a cells (***a***) or inverted images of 8 DIV cortical neurons (***c***) expressing EV, mCtl, or mALID1 are shown. ***b***, ***d***, Three-dimensional deconvolved images were quantified and morphological changes are plotted as relative difference of total neurite area compared with EV or mCtl as described in Materials and Methods. ***e***, Coimmunoprecipitation analysis of mALID1 interaction with $G\alpha_S$ was evaluated in N2a cells transiently cotransfected with EV, mCtl, mAICD, or mALID1 and $G\alpha_S$-wt. Non-denaturing lysates were immunoprecipitated with mAb HA and analyzed by immunoblotting with CT11 to detect tagged mAICD and mALID1. Statistical analysis was performed using ANOVA Kruskal–Wallis test followed by Dunn's *post hoc* multiple-comparison analysis. $^{**}p < 0.001$, compared with EV- or mCtl-expressing cells. The total number of cells quantified, from three independent experiments, is shown in parentheses. Error bars indicate SEM.

### Functional coupling of membrane-targeted APLP1 homolog with $G\alpha_S$-protein

APP possesses two homologs (APLP1 and APLP2) that undergo secretase cleavages similar to APP cleavage releasing also an intracellular cytoplasmic domain (for review, see Aydin et al., 2012; Guo et al., 2012). It has been suggested that these homolog might possess very similar physiological properties based on their structural similarities, which was also supported by gene knockdown studies. Additional studies indicate that APP and its homolog may form heterocomplexes that required the presence of each other to favor their cell-adhesive property (Soba et al., 2005). To determine the selectivity of mAICD-induced neurite outgrowth and associated $G\alpha_S$-protein signaling, we explored the possibility that APLP1 homolog might possess similar property. Indeed, we found that N2a cells and cortical neurons exert as well an increase of neurite outgrowth following expression of APLP1 membrane-tethered intracellular domain (named mALID1; Fig. 9*a–d*). Statistical analysis revealed a significant increase of total neurite area in N2a cells (Fig. 9*a*,*b*; $p < 0.001$) and mouse cortical neurons (Fig. 9*c*,*d*; $p < 0.001$) expressing mALID1 compared with EV- or mCtl-expressing cells. In agreement with these findings, we observed that mALID1 also coimmunoprecipitated with $G\alpha_S$-coupled proteins from non-denaturing lysates of transfected cells (Fig. 9*e*). Collectively, these results strongly support that APLP1-CTF promotes as well neurite outgrowth through its membrane association with $G\alpha_S$-protein coupling.

### Accumulation of APP-CTF through γ-secretase inhibition induces neurite outgrowth

Next, to establish the critical role of APP secretase activity and APP-CTF accumulation in APP function, we first examined neurite outgrowth induced by accumulation of APP-CTF through pharmacological γ-secretase inhibition (Fig. 10*a–d*). As described earlier (Fig. 1*e*,*f*), inhibition of γ-secretase using Compound E stimulated neurite outgrowth in N2a cells and cortical neurons expressing APP-FL. This increase was abrogated by treatment with MDL-12,330A in N2a cells (Fig. 10*a*, bottom; *b*) and cortical neuron cultures (Fig. 10*c*, bottom; *d*). Thus, as in the case of mAICD expression discussed above (Fig. 6), adenylate cyclase activity is required for the activation of neurite outgrowth following accumulation of APP-CTF derived from proteolytic processing of APP-FL (Fig. 10*a–d*).

To substantiate the finding from pharmacological inhibition studies, we performed additional experiments using N2a cells stably expressing an experimental γ-secretase loss-of-function PS1 mutant (PS1-D385A). As expected from previous reports (Wolfe et al., 1999; Vetrivel et al., 2005), stable PS1-D385A cells accumulate higher levels of APP-CTFs compared with stable PS1-wt cells, following transient transfection with APP-FL (Fig. 10*e*). This APP-CTF accumulation parallels an increase of neurite outgrowth (Fig. 10*f*,*g*). Interestingly, expression of APP-C99 (comparable with the level of mAICD expression) was sufficient to induce neurite outgrowth in PS1-wt-expressing cells. Nevertheless, the stimulation of neurite extension following APP-C99

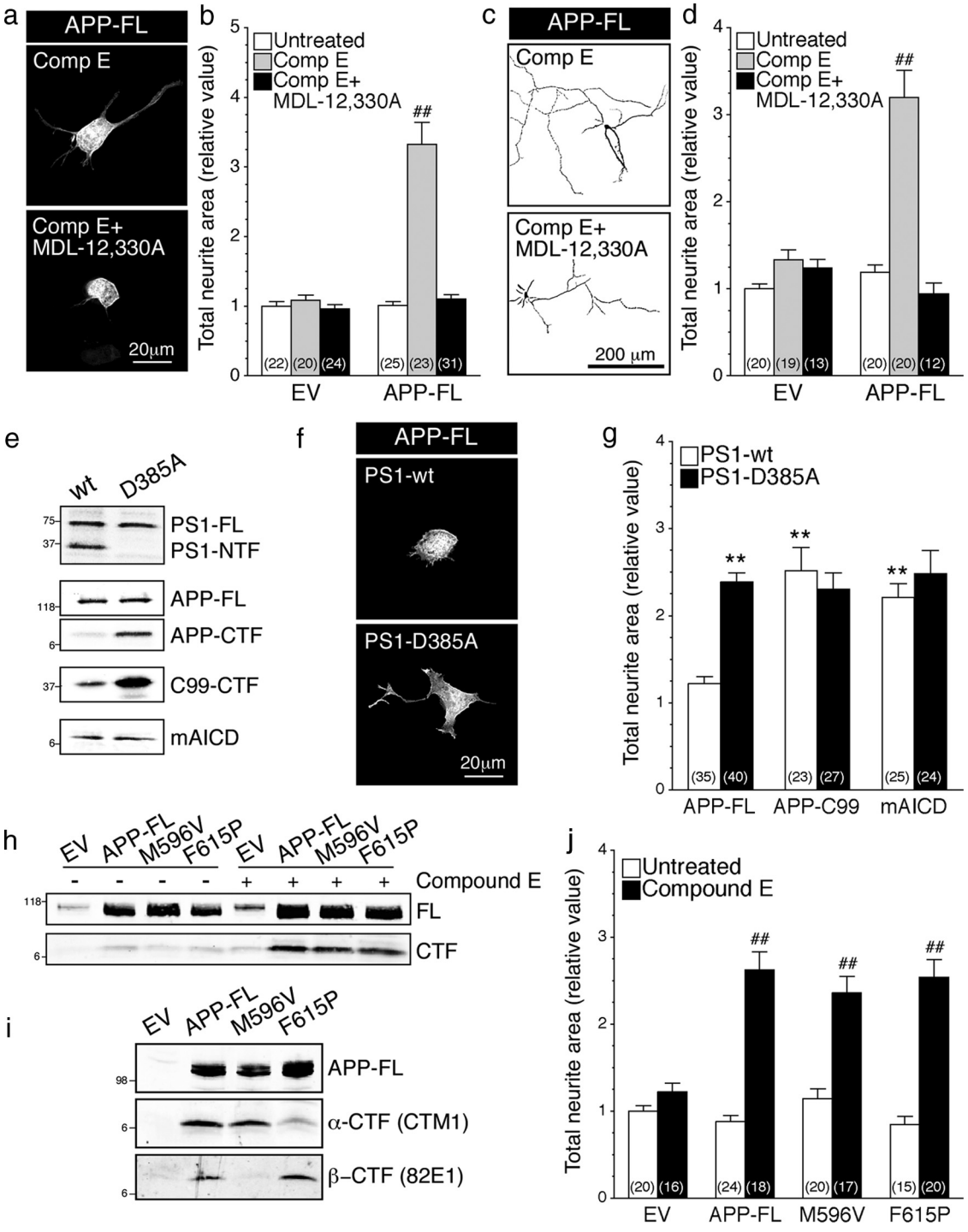


**Figure 10.** Accumulation of APP-CTF through γ-secretase inhibition induce neurite outgrowth. N2a cells and cortical neurons coexpressing YFP and EV or APP-FL were treated with Compound E (10 nM; 24 h) and/or adenylate cyclase inhibitor MDL-12,330A (10 nM; 30 min) and neurite extensions were quantified as described in Materials and Methods. Representative images of N2a cells (***a***) or inverted images of 8 DIV cortical neurons (***c***) coexpressing YFP and APP-FL are shown. ***b***, ***d***, Morphological changes were quantified and plotted relative to untreated EV/YFP cells. ***e–g***, N2a cells stably expressing PS1-wt or PS1-D385A were transiently transfected with EV, APP-FL, APP-C99 – 6myc, or mAICD. ***e***, The levels of PS1 and APP expression were analyzed by Western blotting using PS1NT and CTM1 antibodies, respectively. ***f***, Representative images of N2a cells coexpressing YFP and APP-FL are shown. ***g***, Quantitative analysis of total neurite area relative to EV control cells demonstrated that the loss of PS1 function affects neurite outgrowth in N2a cells. ***h–j***, APP-CTF accumulation through differential secretase processing. N2a cells (***h***, ***j***) and COS cells (***i***) were transiently transfected with EV, APP-FL, APP-M596V (APP β-site cleavage mutant), or APP-F615P (APP α-site cleavage mutant) and treated with or without Compound E (24 h; 10 nM). To detect α- and β-CTFs of APP, Western blotting analysis of Tris-Tricine gels was performed using rabbit polyclonal CTM1 and mouse monoclonal 82E1 antibodies. ***j***, N2a cells were transiently transfected with EV or the indicated APP-FL variants. The total neurite area was quantified and plotted relative to untreated EV cells. Statistical analysis was performed using ANOVA Kruskal–Wallis test followed by Dunn's *post hoc* multiple-comparison analysis. $^{**}p < 0.001$, compared with stable PS1-wt N2a cells expressing APP-FL. $^{\#\#}p < 0.001$, compared with untreated cells or PS1-wt control cells within the same transfected condition. The total number of cells, quantified from at least three independent experiments, is shown in parentheses. Error bars indicate SEM.

transfection was comparable in PS1-wt and D385A cells, despite the relatively higher accumulation of APP-C99 in D385A cells. This observation, along with the data from mAICD with FSK experiments described above, is consistent with the notion that the signaling mediated by APP intracellular domain has reached a point of saturation.

Processing of APP-FL by α- and β-secretases generates α- and β-CTFs, respectively, differing at their extreme N terminus but sharing the same transmembrane and intracellular domains. To test whether accumulation of either α- or β-CTFs differentially regulates neurite extension, we stably expressed APP-FL β-site cleavage mutant (M596V) or APP-FL α-site cleavage mutant (F615P) in N2a cells and examined their effect on neurite outgrowth. As shown in Figure 10*h*, the overall levels of APP-CTFs were comparable in cells expressing wt APP-FL and α- or β-secretase cleavage site mutants at basal levels and following inhibition of γ-secretase activity. However, as expected from previous studies (Sisodia, 1992; Citron et al., 1995; Vetrivel et al., 2011), fractionation of lysates on high-resolution Tris-Tricine gels reveal that β-CTFs were not generated by APP-M596V mutant, whereas APP-F615P mutant generated higher levels of β-CTF at the expense of α-CTF production (Fig. 10*i*). Further analysis of N2a cells revealed that expression of APP-FL wt or APP-FL mutants uniformly stimulated neurite outgrowth following treatment with Compound E (Fig. 10*j*). Collectively, these results indicate that α- or β-secretase processing of APP does not differentially stimulate neurite outgrowth in N2a cells.

## Discussion

In this study, we investigated the potential function of membrane-tethered APP intracellular domain in neurons using a fusion protein mAICD in which the extracellular and transmembrane domains of APP were deleted and replaced by sequences encoding membrane-targeting MyrPalm motif. This strategy allowed us to recruit APP-CTF to lipid raft membrane microdomains, and potentially activate in a constitutive manner putative signaling associated with the APP intracellular domain. We found that accumulation of membrane-tethered APP-CTF, resulting from the inhibition of γ-secretase processing of APP-FL or by expression of mAICD, produced a marked increase of neurite extension in primary cortical neurons, H19-7 hippocampal cells, and N2a neuroblastoma cells. Moreover, we report that membrane accumulation of APP intracellular domain is intimately coupled to adenylate cyclase signaling, which mediates enhanced neurite formation. Our results show that Gα$_S$ coupling to adenylate cyclase is a necessary step in mAICD-induced neurite outgrowth in primary neurons as well as neuronal cell lines. Finally, we demonstrate that a BBXXB motif ($^{672}$RHLSK$^{676}$) within APP-CTF as the functional site of interaction with Gα$_S$-protein and that this interaction is critical to promote neurite extension.

Several reports have previously linked APP expression to neurite outgrowth (Allinquant et al., 1995; Perez et al., 1997; Ando et al., 1999; Small et al., 1999; Leyssen et al., 2005; Young-Pearse et al., 2008; Hoe et al., 2009, 2012). Indeed, cell surface APP, its soluble ectodomain cleavage product, and APP-CTF have been reported to regulate neurite outgrowth. Several mechanisms have been proposed including a role of Aβ/APP receptor-mediated signaling (Ando et al., 1999; Young-Pearse et al., 2008; Shaked et al., 2009; Sola Vigo et al., 2009). The theory that APP may function as a receptor has been proposed based mainly on structural similarity to type I membrane receptors, a concept that has been debated for more than a decade. Indeed, our findings clearly support the idea that APP is acting as a G-protein-coupled receptor, a model in which membrane-bound APP-CTF facilitates interactions and recruitment of cytosolic adaptors and proteins that exacerbate intracellular signaling and influence a variety of cellular functions, including neurite outgrowth (Fig. 11). It was previously reported that APP could interact with Go complex (Nishimoto et al., 1993; Brouillet et al., 1999; Shaked et al., 2009). However, neither report established that the interaction of APP-CTF with Go complex is functional or has direct implications for the developing nervous system. In our study, we outline our characterization of APP with another G-protein-coupled subunit, Gα$_S$. But, most importantly, we demonstrate that interaction of APP-CTF with Gα$_S$ is necessary and sufficient to induce neurite formation in mammalian neurons, ruling out major contribution of other putative G-protein interactions in neurite outgrowth. Using modulators of cAMP/PKA activities, we establish that adenylate cyclase activation plays a pivotal role in APP-CTF-induced neurite outgrowth. Furthermore, our results demonstrate that direct coupling of membrane-bound APP intracellular domain to Gα$_S$ is a previously unrecognized essential step that mediates this function.

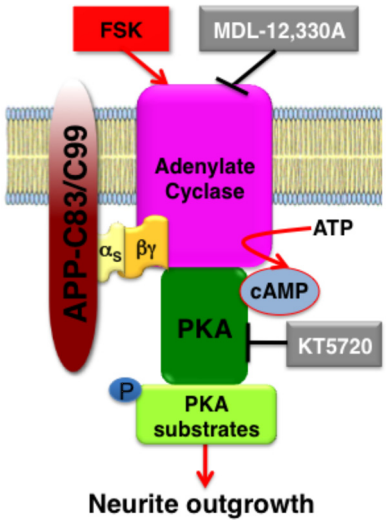


**Figure 11.** G-protein-coupled signaling mediated by membrane-tethered APP intracellular domain. Our results show that accumulation of APP intracellular domain at the membrane initiates intracellular signaling that promotes neurite outgrowth. Membrane-tethered APP intracellular domain interacts with Gα$_S$ through a "BBXXB" motif. This interaction elicits cAMP-dependent signaling cascade in neurons, leading to enhanced phosphorylation of PKA substrates such as CREB and GSK3β and enhanced axonal as well as dendritic arborization in mouse cortical neurons.

Several years ago, it was reported that residues 657–676 of APP cytoplasmic domain (which includes $^{672}$RHLSK$^{676}$ domain) possess affinity for Gα$_O$-protein (also referred to as G$_O$); this interaction was found to activate Gα$_O$-protein reconstituted in phospholipid vesicles with synthetic APP-CTF peptides (Nishimoto et al., 1993). However, a subsequent study reexamined this issue using neuronal membranes prepared from E19 rat embryonic brain tissue and reported that physiological interaction with APP cytoplasmic tail inhibited Gα$_O$ GTPase activity (Brouillet et al., 1999). While both studies identified residues $^{657}$HH$^{658}$ as critical for Gα$_O$ interaction (Nishimoto et al., 1993; Brouillet et al., 1999), neither study examined the functional outcome of APP interaction with Gα$_O$-protein. Nevertheless, based on stimulation or inhibition of Gα$_O$ GTPase activity following the application of mAb22C11, which binds to the extracellular

domain of APP, these studies simply speculated that APP functions as a receptor and $G\alpha_O$-protein binding likely is involved in signal transduction. Therefore, by analogy to other G-protein-coupled receptors such as the adrenergic and serotonergic receptors (Eason et al., 1992; Lefkowitz, 1998; Xiao, 2001; Pindon et al., 2002), it is possible that signaling through APP-CTF involves stochastic or simultaneous binding of $G\alpha_O$ and $G\alpha_S$ on the same APP molecule. Referred to as G-protein coupling "promiscuity," this attribute could indeed account for limiting the spatiotemporal signaling of G-protein-coupled receptors (Woehler and Ponimaskin, 2009). Further studies will be needed to fully understand the complexity of this paradigm with specific emphasis on APP.

G-protein-coupled receptors are known to activate G-proteins from more than one family. Following G-protein-coupled receptor activation, $G\alpha_S$ and $G\alpha_{i/O}$ class of G-proteins mediate stimulation or inhibition of adenylate cyclase activity, respectively. Because expression of mAICD correlated with the activation of adenylate cyclase, we focused our attention on $G\alpha_S$. Our functional study on neurite outgrowth defines BBXXB motif as the binding site for the previously unrecognized $G\alpha_S$ interaction with APP C-terminal domain. The BBXXB motif and sequences with similar characteristics are known to be involved in the G-protein activity of several cell surface membrane receptors (Okamoto et al., 1990; Okamoto and Nishimoto, 1992; Wu et al., 1995; Pauwels et al., 1999; Zhou and Murthy, 2003; Ulloa-Aguirre et al., 2007; Peverelli et al., 2009). Our results also demonstrate that palmitoylation of $G\alpha_S$ is a prerequisite for interaction with the BBXXB motif in APP.

Here, we show that membrane-bound APP intracellular domain regulates neurite formation by G-protein coupling, eliciting adenylate cyclase-dependent intracellular signaling, independent of the transcriptional role ascribed to AICD (Müller et al., 2008; Schettini et al., 2010). Although our studies focused on neurite formation, adenylate cyclase activation resulting from APP-CTF coupling to $G\alpha_S$ could play a critical role in regulating short- and long-term synaptic plasticity (Malenka and Nicoll, 1999; Malinow and Malenka, 2002), and memory formation (Arnsten et al., 2005; Abel and Nguyen, 2008). In support of this idea, we have previously reported increase of synaptic neurotransmission associated with cAMP/PKA pathway activation in presenilin 1-deficient neurons (Parent et al., 2005; Barnes et al., 2008), a condition in which APP-CTF accumulates at the cell surface (Leem et al., 2002; Barnes et al., 2008) and in lipid raft (Vetrivel et al., 2005). More interestingly, our studies show that accumulation of APP-CTF at the membrane produces dual PKA activation and GSK3$\beta$ inhibition in neurons and neuroblastoma cells. Clear evidence in the literature suggests that these dual signaling events would favor axodendritic formation and function (Lonze and Ginty, 2002; Jope and Johnson, 2004; Yoshimura et al., 2006; Hur and Zhou, 2010; Hutchins, 2010; Shelly et al., 2010). GSK3$\beta$ activation is a known pathological hallmark of AD (Hooper et al., 2008; Hernández et al., 2010). Therefore, a relationship between signaling initiated by APP-CTF and GSK3$\beta$ inhibition highlights an aspect that is extremely important as a new perspective to AD etiology and therapeutics.

Further studies are needed to address the possibility that expression of the CTFs derived from APP/APLP homologs might be sufficient to rescue reduced neurite outgrowth and synaptic defects previously reported in APP-deficient neurons (Allinquant et al., 1995; Zheng and Koo, 2006; Hoe et al., 2009, 2012; Lee et al., 2010; Aydin et al., 2012; Guo et al., 2012). Moreover, we need to consider the possibility that lack of APP expression alone might not produce a "loss of function" pertaining to neurite outgrowth downstream of G-protein-coupled signaling mediated by APP/APLPs. To further characterize the physiological relevance of the signaling that we have discovered, study in APP/APLP1 or APP/APLP2 double knock-out neurons could be necessary. Still, much needs to be learned regarding the subcellular sites where APP-CTFs reside and function in $G\alpha_S$ signaling in neurons before the intracellular domain is released from the membrane by $\gamma$-secretase processing. For example, a recent study showed that synaptic activity only regulates processing of a subset of APP-CTFs in Arc-containing endosomes in dendritic structures (Wu et al., 2011). Therefore, although we used neurite outgrowth as our assay in the overexpression experiments, the physiological functions regulated by APP/APLP-CTF signaling through $G\alpha_S$ coupling in neurons could be subtler to discern.

In recent years, G-protein-coupled receptor signaling cascades have been proposed as a therapeutic target for AD by several investigators (for review, see Thathiah and De Strooper, 2011). Therefore, the novel functional coupling of APP-CTF with $G\alpha_S$-protein at the neuronal membrane identified in this study has important implications because accumulation of APP-CTF at the membrane is an invariable outcome of therapeutic inhibition of $\gamma$-secretase processing of APP aimed at reducing cerebral amyloid burden.

## References


Abel T, Nguyen PV (2008) Regulation of hippocampus-dependent memory by cyclic AMP-dependent protein kinase. Prog Brain Res 169:97–115.

Abramoff MD, Magelhaes PJ, Ram SJ (2004) Image processing with ImageJ. Biophotonics Int 11:36–42.

Allen JA, Halverson-Tamboli RA, Rasenick MM (2007) Lipid raft microdomains and neurotransmitter signalling. Nat Rev Neurosci 8:128–140.

Allinquant B, Hantraye P, Mailleux P, Moya K, Bouillot C, Prochiantz A (1995) Downregulation of amyloid precursor protein inhibits neurite outgrowth in vitro. J Cell Biol 128:919–927.

Ando K, Oishi M, Takeda S, Iijima K, Isohara T, Nairn AC, Kirino Y, Greengard P, Suzuki T (1999) Role of phosphorylation of Alzheimer's amyloid precursor protein during neuronal differentiation. J Neurosci 19:4421–4427.

Arnsten AF, Ramos BP, Birnbaum SG, Taylor JR (2005) Protein kinase A as a therapeutic target for memory disorders: rationale and challenges. Trends Mol Med 11:121–128.

Aydin D, Weyer SW, Muller UC (2012) Functions of the APP gene family in the nervous system: insights from mouse models. Exp Brain Res. Advance online publication. Retrieved January 4, 2012. doi:10.1007/s00221-011-2861-2.

Barnes NY, Shi J, Yajima H, Thinakaran G, Parent AT (2008) Steady-state increase of cAMP-response element binding protein, Rac, and PAK signaling in presenilin-deficient neurons. J Neurochem 104:1637–1648.

Biederer T, Cao X, Südhof TC, Liu X (2002) Regulation of APP-dependent transcription complexes by Mint/X11s: differential functions of Mint isoforms. J Neurosci 22:7340–7351.

Brouillet E, Trembleau A, Galanaud D, Volovitch M, Bouillot C, Valenza C, Prochiantz A, Allinquant B (1999) The amyloid precursor protein interacts with Go heterotrimeric protein within a cell compartment specialized in signal transduction. J Neurosci 19:1717–1727.

Cheng H, Vetrivel KS, Gong P, Meckler X, Parent A, Thinakaran G (2007) Mechanisms of disease: new therapeutic strategies for Alzheimer's disease—targeting APP processing in lipid rafts. Nat Clin Pract Neurol 3:374–382.

Citron M, Teplow DB, Selkoe DJ (1995) Generation of amyloid beta protein from its precursor is sequence specific. Neuron 14:661–670.

Deyts C, Galan-Rodriguez B, Martin E, Bouveyron N, Roze E, Charvin D, Caboche J, Bétuing S (2009) Dopamine $D_2$ receptor stimulation potentiates PolyQ-Huntingtin-induced mouse striatal neuron dysfunctions via Rho/ROCK-II activation. PLoS One 4:e8287.

Dupré DJ, Robitaille M, Richer M, Ethier N, Mamarbachi AM, Hébert TE (2007) Dopamine receptor-interacting protein 78 acts as a molecular chaperone for Ggamma subunits before assembly with Gbeta. J Biol Chem 282:13703–13715.

Eason MG, Kurose H, Holt BD, Raymond JR, Liggett SB (1992) Simultaneous coupling of alpha 2-adrenergic receptors to two G-proteins with opposing

effects. Subtype-selective coupling of alpha 2C10, alpha 2C4, and alpha 2C2 adrenergic receptors to Gi and Gs. J Biol Chem 267:15795–15801.

Eves EM, Tucker MS, Roback JD, Downen M, Rosner MR, Wainer BH (1992) Immortal rat hippocampal cell lines exhibit neuronal and glial lineages and neurotrophin gene expression. Proc Natl Acad Sci U S A 89:4373–4377.

Fang X, Yu SX, Lu Y, Bast RC Jr, Woodgett JR, Mills GB (2000) Phosphorylation and inactivation of glycogen synthase kinase 3 by protein kinase A. Proc Natl Acad Sci U S A 97:11960–11965.

Ginty DD, Kornhauser JM, Thompson MA, Bading H, Mayo KE, Takahashi JS, Greenberg ME (1993) Regulation of CREB phosphorylation in the suprachiasmatic nucleus by light and a circadian clock. Science 260:238–241.

Gong P, Vetrivel KS, Nguyen PD, Meckler X, Cheng H, Kounnas MZ, Wagner SL, Parent AT, Thinakaran G (2010) Mutation analysis of the presenilin 1 N-terminal domain reveals a broad spectrum of gamma-secretase activity toward amyloid precursor protein and other substrates. J Biol Chem 285:38042–38052.

Grønborg M, Kristiansen TZ, Stensballe A, Andersen JS, Ohara O, Mann M, Jensen ON, Pandey A (2002) A mass spectrometry-based proteomic approach for identification of serine/threonine-phosphorylated proteins by enrichment with phospho-specific antibodies: identification of a novel protein, Frigg, as a protein kinase A substrate. Mol Cell Proteomics 1:517–527.

Guo Q, Wang Z, Li H, Wiese M, Zheng H (2012) APP physiological and pathophysiological functions: insights from animal models. Cell Res. 22:78–89.

Hernández F, Gómez de Barreda E, Fuster-Matanzo A, Lucas JJ, Avila J (2010) GSK3: a possible link between beta amyloid peptide and tau protein. Exp Neurol 223:322–325.

Hoe HS, Lee KJ, Carney RS, Lee J, Markova A, Lee JY, Howell BW, Hyman BT, Pak DT, Bu G, Rebeck GW (2009) Interaction of reelin with amyloid precursor protein promotes neurite outgrowth. J Neurosci 29:7459–7473.

Hoe HS, Lee HK, Pak DT (2012) The upside of APP at synapses. CNS Neurosci Ther. Advance online publication. Retrieved January 4, 2012. doi:10.1111/j.1755-5949.2010.00221.x.

Hooper C, Killick R, Lovestone S (2008) The GSK3 hypothesis of Alzheimer's disease. J Neurochem 104:1433–1439.

Hur EM, Zhou FQ (2010) GSK3 signalling in neural development. Nat Rev Neurosci 11:539–551.

Hutchins BI (2010) Competitive outgrowth of neural processes arising from long-distance cAMP signaling. Sci Signal 3:jc1.

Jope RS, Johnson GV (2004) The glamour and gloom of glycogen synthase kinase-3. Trends Biochem Sci 29:95–102.

Lee KJ, Moussa CE, Lee Y, Sung Y, Howell BW, Turner RS, Pak DT, Hoe HS (2010) Beta amyloid-independent role of amyloid precursor protein in generation and maintenance of dendritic spines. Neuroscience 169:344–356.

Leem JY, Saura CA, Pietrzik C, Christianson J, Wanamaker C, King LT, Veselits ML, Tomita T, Gasparini L, Iwatsubo T, Xu H, Green WN, Koo EH, Thinakaran G (2002) A role for presenilin 1 in regulating the delivery of amyloid precursor protein to the cell surface. Neurobiol Dis 11: 64–82.

Lefkowitz RJ (1998) G protein-coupled receptors. III. New roles for receptor kinases and beta-arrestins in receptor signaling and desensitization. J Biol Chem 273:18677–18680.

Leyssen M, Ayaz D, Hébert SS, Reeve S, De Strooper B, Hassan BA (2005) Amyloid precursor protein promotes post-developmental neurite arborization in the *Drosophila* brain. EMBO J 24:2944–2955.

Lichtenthaler SF, Haass C, Steiner H (2011) Regulated intramembrane proteolysis—lessons from amyloid precursor protein processing. J Neurochem 117:779–796.

Lonze BE, Ginty DD (2002) Function and regulation of CREB family transcription factors in the nervous system. Neuron 35:605–623.

Malenka RC, Nicoll RA (1999) Long-term potentiation—a decade of progress? Science 285:1870–1874.

Malinow R, Malenka RC (2002) AMPA receptor trafficking and synaptic plasticity. Annu Rev Neurosci 25:103–126.

Müller T, Meyer HE, Egensperger R, Marcus K (2008) The amyloid precursor protein intracellular domain (AICD) as modulator of gene expression, apoptosis, and cytoskeletal dynamics-relevance for Alzheimer's disease. Prog Neurobiol 85:393–406.

Nishimoto I, Okamoto T, Matsuura Y, Takahashi S, Okamoto T, Murayama Y, Ogata E (1993) Alzheimer amyloid protein precursor complexes with brain GTP-binding protein $G_o$. Nature 362:75–79.

Okamoto T, Nishimoto I (1992) Detection of G protein-activator regions in M4 subtype muscarinic, cholinergic, and alpha 2-adrenergic receptors based upon characteristics in primary structure. J Biol Chem 267:8342–8346.

Okamoto T, Katada T, Murayama Y, Ui M, Ogata E, Nishimoto I (1990) A simple structure encodes G protein-activating function of the IGF-II/mannose 6-phosphate receptor. Cell 62:709–717.

Onishi M, Kinoshita S, Morikawa Y, Shibuya A, Phillips J, Lanier LL, Gorman DM, Nolan GP, Miyajima A, Kitamura T (1996) Applications of retrovirus-mediated expression cloning. Exp Hematol 24:324–329.

Parent AT, Barnes NY, Taniguchi Y, Thinakaran G, Sisodia SS (2005) Presenilin attenuates receptor-mediated signaling and synaptic function. J Neurosci 25:1540–1549.

Pauwels PJ, Gouble A, Wurch T (1999) Activation of constitutive 5-hydroxytryptamine(1B) receptor by a series of mutations in the BBXXB motif: positioning of the third intracellular loop distal junction and its $G_o$alpha protein interactions. Biochem J 343:435–442.

Perez RG, Zheng H, Van der Ploeg LH, Koo EH (1997) The beta-amyloid precursor protein of Alzheimer's disease enhances neuron viability and modulates neuronal polarity. J Neurosci 17:9407–9414.

Peverelli E, Lania AG, Mantovani G, Beck-Peccoz P, Spada A (2009) Characterization of intracellular signaling mediated by human somatostatin receptor 5: role of the DRY motif and the third intracellular loop. Endocrinology 150:3169–3176.

Pindon A, van Hecke G, van Gompel P, Lesage AS, Leysen JE, Jurzak M (2002) Differences in signal transduction of two 5-$HT_4$ receptor splice variants: compound specificity and dual coupling with Galphas- and Galphai/o-proteins. Mol Pharmacol 61:85–96.

Sanchez S, Sayas CL, Lim F, Diaz-Nido J, Avila J, Wandosell F (2001) The inhibition of phosphatidylinositol-3-kinase induces neurite retraction and activates GSK3. J Neurochem 78:468–481.

Schettini G, Govoni S, Racchi M, Rodriguez G (2010) Phosphorylation of APP-CTF-AICD domains and interaction with adaptor proteins: signal transduction and/or transcriptional role—relevance for Alzheimer pathology. J Neurochem 115:1299–1308.

Seiffert D, Bradley JD, Rominger CM, Rominger DH, Yang F, Meredith JE Jr, Wang Q, Roach AH, Thompson LA, Spitz SM, Higaki JN, Prakash SR, Combs AP, Copeland RA, Arneric SP, Hartig PR, Robertson DW, Cordell B, Stern AM, Olson RE, et al. (2000) Presenilin-1 and -2 are molecular targets for gamma-secretase inhibitors. J Biol Chem 275:34086–34091.

Shaked GM, Chauv S, Ubhi K, Hansen LA, Masliah E (2009) Interactions between the amyloid precursor protein C-terminal domain and G proteins mediate calcium dysregulation and amyloid beta toxicity in Alzheimer's disease. FEBS J 276:2736–2751.

Shelly M, Lim BK, Cancedda L, Heilshorn SC, Gao H, Poo MM (2010) Local and long-range reciprocal regulation of cAMP and cGMP in axon/dendrite formation. Science 327:547–552.

Sisodia SS (1992) Beta-amyloid precursor protein cleavage by a membrane-bound protease. Proc Natl Acad Sci U S A 89:6075–6079.

Small DH, Clarris HL, Williamson TG, Reed G, Key B, Mok SS, Beyreuther K, Masters CL, Nurcombe V (1999) Neurite-outgrowth regulating functions of the amyloid protein precursor of Alzheimer's disease. J Alzheimers Dis 1:275–285.

Soba P, Eggert S, Wagner K, Zentgraf H, Siehl K, Kreger S, Löwer A, Langer A, Merdes G, Paro R, Masters CL, Müller U, Kins S, Beyreuther K (2005) Homo- and heterodimerization of APP family members promotes intercellular adhesion. EMBO J 24:3624–3634.

Sola Vigo F, Kedikian G, Heredia L, Heredia F, Añel AD, Rosa AL, Lorenzo A (2009) Amyloid-beta precursor protein mediates neuronal toxicity of amyloid beta through Go protein activation. Neurobiol Aging 30:1379–1392.

Suzuki T, Nakaya T (2008) Regulation of amyloid beta-protein precursor by phosphorylation and protein interactions. J Biol Chem 283:29633–29637.

Thathiah A, De Strooper B (2011) The role of G protein-coupled receptors in the pathology of Alzheimer's disease. Nat Rev Neurosci 12:73–87.

Thinakaran G, Koo EH (2008) Amyloid precursor protein trafficking, processing, and function. J Biol Chem 283:29615–29619.

Thinakaran G, Regard JB, Bouton CM, Harris CL, Price DL, Borchelt DR,

Sisodia SS (1998) Stable association of presenilin derivatives and absence of presenilin interactions with APP. Neurobiol Dis 4:438–453.
Turner PR, O'Connor K, Tate WP, Abraham WC (2003) Roles of amyloid precursor protein and its fragments in regulating neural activity, plasticity and memory. Prog Neurobiol 70:1–32.
Ulloa-Aguirre A, Uribe A, Zarinan T, Bustos-Jaimes I, Perez-Solis MA, Dias JA (2007) Role of the intracellular domains of the human FSH receptor in G(alphaS) protein coupling and receptor expression. Mol Cell Endocrinol 260–262:153–162.
Vetrivel KS, Cheng H, Lin W, Sakurai T, Li T, Nukina N, Wong PC, Xu H, Thinakaran G (2004) Association of gamma-secretase with lipid rafts in post-Golgi and endosome membranes. J Biol Chem 279:44945–44954.
Vetrivel KS, Cheng H, Kim SH, Chen Y, Barnes NY, Parent AT, Sisodia SS, Thinakaran G (2005) Spatial segregation of gamma-secretase and substrates in distinct membrane domains. J Biol Chem 280:25892–25900.
Vetrivel KS, Zhang X, Meckler X, Cheng H, Lee S, Gong P, Lopes KO, Chen Y, Iwata N, Yin KJ, Lee JM, Parent AT, Saido TC, Li YM, Sisodia SS, Thinakaran G (2008) Evidence that CD147 modulation of beta-amyloid (Abeta) levels is mediated by extracellular degradation of secreted Abeta. J Biol Chem 283:19489–19498.
Vetrivel KS, Meckler X, Chen Y, Nguyen PD, Seidah NG, Vassar R, Wong PC, Fukata M, Kounnas MZ, Thinakaran G (2009) Alzheimer disease Abeta production in the absence of S-palmitoylation-dependent targeting of BACE1 to lipid rafts. J Biol Chem 284:3793–3803.
Vetrivel KS, Barman A, Chen Y, Nguyen PD, Wagner SL, Prabhakar R, Thinakaran G (2011) Loss of cleavage at $\beta'$-site contributes to apparent increase in $\beta$-amyloid peptide (A$\beta$) secretion by $\beta$-secretase (BACE1)-glycosylphosphatidylinositol (GPI) processing of amyloid precursor protein. J Biol Chem 286:26166–26177.
von Koch CS, Zheng H, Chen H, Trumbauer M, Thinakaran G, van der Ploeg LH, Price DL, Sisodia SS (1997) Generation of APLP2 KO mice and early postnatal lethality in APLP2/APP double KO mice. Neurobiol Aging 18:661–669.
Wedegaertner PB, Chu DH, Wilson PT, Levis MJ, Bourne HR (1993) Palmitoylation is required for signaling functions and membrane attachment of Gq alpha and Gs alpha. J Biol Chem 268:25001–25008.
Woehler A, Ponimaskin EG (2009) G protein-mediated signaling: same receptor, multiple effectors. Curr Mol Pharmacol 2:237–248.
Wolfe MS, Xia W, Ostaszewski BL, Diehl TS, Kimberly WT, Selkoe DJ (1999) Two transmembrane aspartates in presenilin-1 required for presenilin endoproteolysis and gamma-secretase activity. Nature 398:513–517.
Wu D, Jiang H, Simon MI (1995) Different alpha 1-adrenergic receptor sequences required for activating different G alpha subunits of Gq class of G proteins. J Biol Chem 270:9828–9832.
Wu J, Petralia RS, Kurushima H, Patel H, Jung MY, Volk L, Chowdhury S, Shepherd JD, Dehoff M, Li Y, Kuhl D, Huganir RL, Price DL, Scannevin R, Troncoso JC, Wong PC, Worley PF (2011) Arc/Arg3.1 regulates an endosomal pathway essential for activity-dependent beta-amyloid generation. Cell 147:615–628.
Wu X, Zagranichnaya TK, Gurda GT, Eves EM, Villereal ML (2004) A TRPC1/TRPC3-mediated increase in store-operated calcium entry is required for differentiation of H19-7 hippocampal neuronal cells. J Biol Chem 279:43392–43402.
Xiao RP (2001) Beta-adrenergic signaling in the heart: dual coupling of the beta2-adrenergic receptor to $G_s$ and $G_i$ proteins. Sci STKE 2001:re15.
Yoshimura T, Arimura N, Kaibuchi K (2006) Signaling networks in neuronal polarization. J Neurosci 26:10626–10630.
Young-Pearse TL, Chen AC, Chang R, Marquez C, Selkoe DJ (2008) Secreted APP regulates the function of full-length APP in neurite outgrowth through interaction with integrin beta1. Neural Dev 3:15.
Zacharias DA, Violin JD, Newton AC, Tsien RY (2002) Partitioning of lipid-modified monomeric GFPs into membrane microdomains of live cells. Science 296:913–916.
Zheng H, Koo EH (2006) The amyloid precursor protein: beyond amyloid. Mol Neurodegener 1:5.
Zhou H, Murthy KS (2003) Identification of the G protein-activating sequence of the single-transmembrane natriuretic peptide receptor C (NPR-C). Am J Physiol Cell Physiol 284:C1255–C1261.